

SEARCH FOR SURVIVING COMPANIONS OF PROGENITORS OF YOUNG LMC TYPE IA SUPERNOVA REMNANTS

CHUAN-JUI LI (李傳睿)^{1,2}, WOLFGANG E. KERZENDORF³, YOU-HUA CHU (朱有花)^{2,4},
TING-WAN CHEN (陳婷琬)⁵, TUAN DO⁶, ROBERT A. GRUENDL⁴, ABIGAIL HOLMES⁴,
R. ISHIOKA², BRUNO LEIBUNDGUT³, KUO-CHUAN PAN (潘國全)⁷, PAUL M. RICKER⁴, DANIEL WEISZ⁸

¹ Graduate Institute of Astrophysics, National Taiwan University, Taipei 10617, Taiwan, R.O.C.

² Institute of Astronomy and Astrophysics, Academia Sinica, P.O. Box 23-141, Taipei 10617, Taiwan, R.O.C.
cjli@asiaa.sinica.edu.tw, yhchu@asiaa.sinica.edu.tw

³ European Southern Observatory, Karl-Schwarzschild-Straße 2, 85748 Garching bei München, Germany

⁴ Department of Astronomy, University of Illinois at Urbana-Champaign, 1002 West Green Street,
Urbana, IL 61801, U.S.A.

⁵ Max-Planck-Institut für Extraterrestrische Physik, Giessenbachstraße 1, 85748, Garching, Germany

⁶ Physics and Astronomy Department, University of California, Los Angeles, CA 90095-1547, USA

⁷ Department of Physics and Institute of Astronomy, National Tsing Hua University, Hsinchu 30013, Taiwan, R.O.C.

⁸ Department of Astronomy, University of California, 501 Campbell Hall #3411, Berkeley, CA 94720-3411, U.S.A.

Draft version January 27, 2022

ABSTRACT

We have used two methods to search for surviving companions of Type Ia supernova progenitors in three Balmer-dominated supernova remnants (SNRs) in the Large Magellanic Cloud: 0519–69.0, 0505–67.9 (DEML71), and 0548–70.4. In the first method, we use the *Hubble Space Telescope* photometric measurements of stars to construct color-magnitude diagrams (CMDs), and compare positions of stars in the CMDs with those expected from theoretical post-impact evolution of surviving main sequence or helium star companions. No obvious candidates of surviving companion are identified in this photometric search. Future models for surviving red giant companions or with different explosion mechanisms are needed for thorough comparisons with these observations in order to make more definitive conclusions. In the second method, we use Multi-Unit Spectroscopic Explorer (MUSE) observations of 0519–69.0 and DEML71 to carry out spectroscopic analyses of stars in order to use large peculiar radial velocities as diagnostics of surviving companions. We find a star in 0519–69.0 and a star in DEML71 moving at radial velocities of $182 \pm 0 \text{ km s}^{-1}$ and $213 \pm 0 \text{ km s}^{-1}$, more than 2.5σ from the mean radial velocity of the underlying stellar population, 264 km s^{-1} and 270 km s^{-1} , respectively. These stars need higher-quality spectra to investigate their abundances and rotation velocities to determine whether they are indeed surviving companions of the SN progenitors.

Subject headings: ISM: supernova remnants — Magellanic Clouds — ISM: individual (SNR 0519–69.0, SNR DEML71, SNR 0548–70.4)

1. INTRODUCTION

Type Ia Supernovae (SNe Ia) are important standardizable candles for determining cosmological distances. While they are known to be thermonuclear explosions of carbon-oxygen white dwarfs (WDs) that have reached \sim the Chandrasekhar mass limit, the exact origins of their progenitor systems are uncertain (see Wang & Han 2012; Maoz et al. 2014; Ruiz-Lapuente 2014; Wang 2018; Ruiz-Lapuente 2018a for reviews). Two contrasting origins have been suggested: a double degenerate (DD) origin that results from the merger of two WDs (Iben & Tutukov 1984; Webbink 1984), and a single degenerate (SD) origin in which a WD accretes material from a non-degenerate companion (Whelan & Iben 1973; Nomoto 1982).

In the DD case, both WDs are destroyed and no stellar remnant is expected. In the SD case, the non-degenerate companion may be a main-sequence (MS) star (Ivanova & Taam 2004; Wang & Han 2010), a red giant (RG) (Hachisu et al. 1999, 2008), or a helium star (Wang & Han 2009; Bildsten et al. 2007); the companion’s surface material may be stripped by the SN blast but its dense core can survive. Surviving companions may be spec-

troscopically identified by distinguishing characteristics, such as high translational velocities, high rotational velocities, and elevated metallicities (Ruiz-Lapuente et al. 2004; González Hernández et al. 2009, 2012; Kerzendorf et al. 2014). Surviving companions may also be identified photometrically through their positions in the color-magnitude diagrams (CMDs) in comparison with models of the post-impact evolution of surviving companions (e.g., Marietta et al. 2000; Pan et al. 2014). If a surviving companion is identified near the explosion center of a young Type Ia supernova remnant (SNR), a SD origin can be affirmed (Ruiz-Lapuente 1997; Canal et al. 2001).

Type Ia SN progenitors’ surviving companions have been searched for in Galactic SNRs Tycho (Ruiz-Lapuente et al. 2004; Fuhrmann 2005; Ihara et al. 2007; Kerzendorf et al. 2009; González Hernández et al. 2009; Kerzendorf et al. 2013; Bedin et al. 2014; Kerzendorf et al. 2018b; Ruiz-Lapuente et al. 2019), SN 1006 (González Hernández et al. 2012; Kerzendorf et al. 2012, 2018a), and Kepler (Kerzendorf et al. 2014; Ruiz-Lapuente et al. 2018b); however, none have been unambiguously identified near explosion centers of these SNRs. Instead, a dense circumstellar medium (CSM) is detected in the SNR Kepler, and this dense CSM has been used to argue

TABLE 1
HST OBSERVATIONS

SNR	R.A.	Decl.	Filter	Instrument	Date	t_{exp} (s)	PI	Proposal ID
0519–69.0	5:19:34.80	-69:02:09.54	F550M	ACS/WFC	2011 Apr 21	750	Hughes	12017
			F658N	ACS/WFC	2011 Apr 21	4757	Hughes	12017
			F475W	WFC3/UVIS	2014 Feb 21	1070	Chu	13282
			F814W	WFC3/UVIS	2014 Feb 21	1174	Chu	13282
DEM L71	5:05:41.70	-67:52:39.90	F475W	WFC3/UVIS	2014 Mar 04	1050	Chu	13282
			F555W	WFC3/UVIS	2014 Mar 04	1117	Chu	13282
			F656N	WFC3/UVIS	2014 Mar 05	1350	Chu	13282
			F814W	WFC3/UVIS	2014 Mar 05	1050	Chu	13282
0548–70.4	5:47:48.50	-70:24:53.32	F475W	WFC3/UVIS	2013 Sep 20	1050	Chu	13282
			F555W	WFC3/UVIS	2013 Sep 20	1170	Chu	13282
			F656N	WFC3/UVIS	2013 Sep 20	1350	Chu	13282
			F814W	WFC3/UVIS	2013 Sep 20	1111	Chu	13282

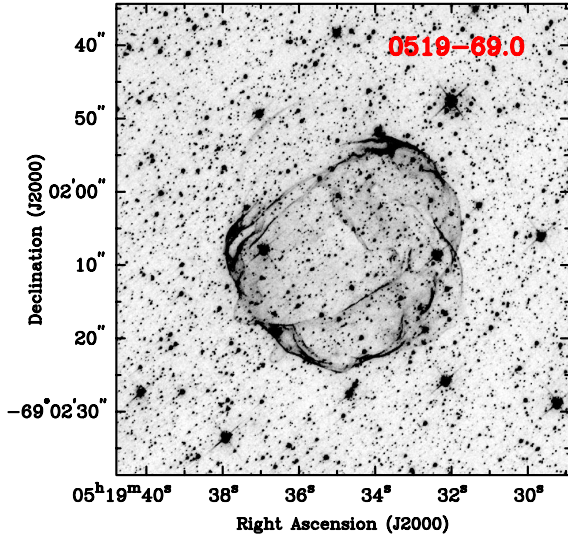


FIG. 1.— High-resolution H α (F658N) image of SNR 0519–69.0 obtained with the *HST* ACS/WFC.

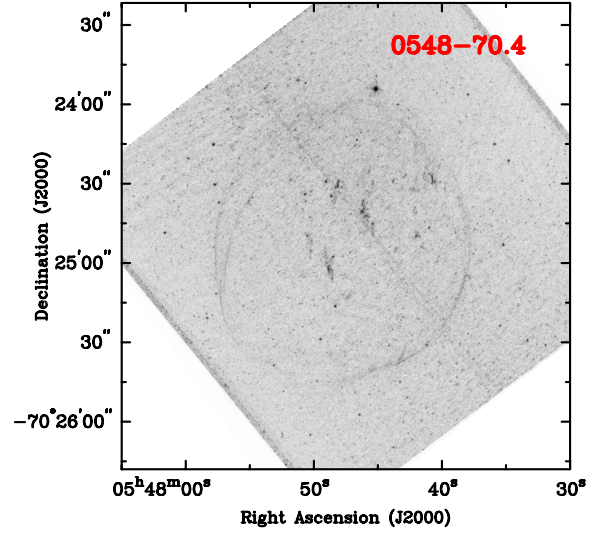


FIG. 3.— High-resolution H α (F656N) image of SNR 0548–70.4 obtained with the *HST* WFC3/UVIS.

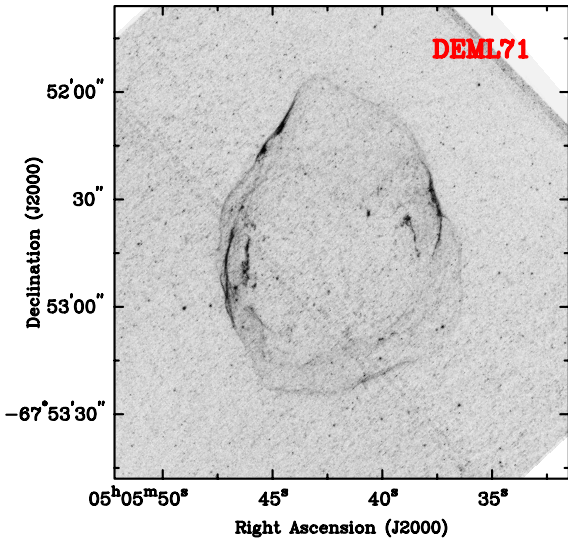


FIG. 2.— High-resolution H α (F656N) image of DEM L71 obtained with the *HST* WFC3/UVIS.

for a SD origin, as it represents mass loss from the binary system of the SN progenitor (Van den Bergh et al. 1973; Van den Bergh & Kamper 1977; Dennefeld 1982; Blair et al. 1991; Williams et al. 2012). From X-ray studies, around 8–9 Type Ia SNRs are known in our Galaxy (Yamaguchi et al. 2014; Martínez-Rodríguez et al. 2018), though only a smaller sample of those are suitable for searches of SN progenitors' surviving companions. Both the identification of Type Ia SNRs and the search for their SN progenitors' surviving companions in the Galaxy are hampered by the confusion and extinction in the Galactic plane, compounded by the uncertain distances to the SNRs.

The Large Magellanic Cloud (LMC), on the other hand, is an ideal galaxy where we can study SNRs (Ou et al. 2018) and search for surviving companions of SN progenitors because it has a large sample of SNRs all at a known moderate distance, ~ 50 kpc (Pietrzyński et al. 2013, 2019), near enough for stars and SNRs to be easily resolved by the *Hubble Space Telescope* (*HST*). Furthermore, confusion and extinction along the lines of sight are minimized by the LMC disk's nearly face-on orientation (Nikolaev et al. 2004; Olsen & Salyk 2002; van der Marel & Cioni 2001; Zaritsky et al. 2004). Searches for surviving companions have been conducted for 4 young Type

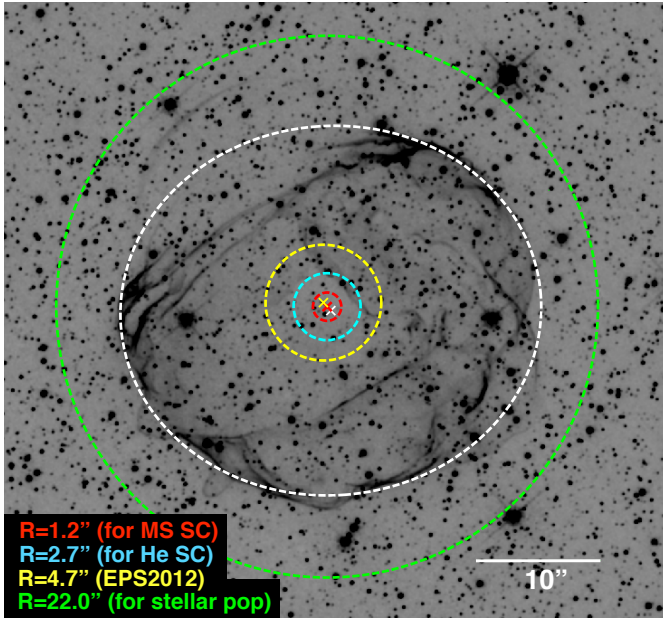


FIG. 4.— $H\alpha$ image of SNR 0519-69.0. The white cross marks the center of the fitted Balmer-dominated ellipse (dashed white), the yellow cross marks the site of SN explosion of EPS2012, and the red cross mark our adopted site of SN explosion, at $05^h19^m34^s.77$, $-69^\circ02'07''.25$ (J2000). The dashed red circle illustrates the maximum projected runaway distance for an MS surviving companion, and the dashed cyan circle represent the maximum projected runaway distance for a helium star surviving companion; the dashed yellow circle marks the search radius of EPS2012. The stars within $22''$ from the center are used to study the background stellar population (the dashed green circle).

Ia SNRs in the LMC: 0509-67.5, 0519-69.0, 0505-67.9 (DEML71), and 0509-68.7 (N103B). As summarized below, no surviving companion has been unambiguously identified and confirmed.

SNR 0509-67.5: This remnant is 400 ± 50 yr old based on analyses of the light echoes of its SN (Rest et al. 2005, 2008). *HST* images reveal a patch of diffuse emission with a point-like central source near the explosion center of this SNR more prominently in the red and near-IR bands than in the blue bands (Litke et al. 2017). The Gemini GMOS long-slit spectrum of this patch shows one emission line and it is identified as $H\alpha$ line at $z \sim 0.03$ (Pagnotta et al. 2014); however, based on the spectral energy distribution of this diffuse patch and absence of other nebular lines, Litke et al. (2017) conclude that the diffuse patch is a background galaxy at $z \sim 0.8$ and that the central point-like source is the nucleus/bulge. Based on comparisons of stars with post-impact evolution models of Pan et al. (2014), Litke et al. (2017) concur with the conclusion of Pagnotta et al. (2014) and Schaefer et al. (2012) that the SN progenitor of 0509-67.5 has no surviving companion.

SNR 0519-69.0: This remnant is 600 ± 200 yr old based on the light echoes of its SN (Rest et al. 2005). Edwards et al. (2012, hereafter EPS2012) use *HST* F550M (V band) and F656N ($H\alpha$ line) images of this SNR to exclude post-main sequence companion, but not MS companion, for the SN progenitor, and further suggest that the SN progenitor was either a supersoft source (Hachisu et al. 1999; Langer et al. 2000; Han & Podsiadlowski 2004) or a DD system.

SNR 0505-67.9 (DEML71): This remnant is more commonly called DEML71 (Davies et al. 1976). Its age

TABLE 2
MUSE OBSERVATIONS

SNR	PI	Program ID	Date	t_{exp} (s)
0519-69.0	Leibundgut	096.D-0352(A)	2016 Jan 17	900
DEM L71	Leibundgut	096.D-0352(A)	2015 Nov 16	900

estimated from size and shock velocity is 4360 ± 290 yr (Ghavamian et al. 2003). Pagnotta & Schaefer (2015, hereafter PS2015) use *Chandra* observations (Hughes et al. 2003; Rakowski et al. 2003) to assess the SNR boundary and explosion center and use Gemini GMOS g' , r' , i' , and $H\alpha$ images to select a large number of possible candidates for the SN's surviving companion; however, none has been confirmed.

SNR 0509-68.7 (N103B): This remnant's age estimated from the SN light echoes is ~ 860 yr (Rest et al. 2005). A SD origin has been suggested because a dense CSM is detected in the remnant (Williams et al. 2014; Li et al. 2017). PS2015 used radio (Dickel & Milne 1995) and X-ray observations (Lewis et al. 2003) to determine the site of the SN explosion, then obtained Gemini GMOS images to examine the stars and found eight candidates for the surviving companion. Alternatively, Li et al. (2017) used the Balmer-dominated filamentary shell, revealed by *HST* $H\alpha$ image, as the fronts of the collisionless shocks to determine the explosion center, and found fifteen stars within 1 pc from the explosion center. They further suggest that the star closest to the explosion center is the most likely candidate for the surviving companion of the SN progenitor, as its location in the CMDs is similar to that expected from a post-impact $\sim 1 M_\odot$ subgiant modeled by Podsiadlowski (2003).

A detailed, up-to-date compilation of methods and results of searches (including this work) for surviving companions in Galactic and LMC Type Ia SNRs is given in Appendix A.

To investigate surviving companions of Type Ia SNe in the LMC, we have obtained new *HST* images in continuum and $H\alpha$ bands for nine Type Ia SNRs in the LMC. We have reported our study of the SNR 0509-67.5 (Litke et al. 2017) and N103B (Li et al. 2017). In this paper, we report our investigation of surviving companions in the other three Balmer-dominated young Type Ia SNRs: 0519-69.0, 0505-67.9 (DEML71), and 0548-70.4 (see Figures 1, 2 and 3). The observations used in this study are described in Section 2. The methodology is detailed in Section 3. Sections 4-6 report our investigation of the three SNRs, respectively. The results are discussed in Section 7, and a summary is given in Section 8.

2. OBSERVATIONS AND DATA REDUCTION

2.1. Hubble Space Telescope Observations

We have obtained new *HST* images of SNR 0519-69.0, DEML71, and SNR 0548-70.4, using the UVIS channel of Wide Field Camera 3 (WFC3) in Program 13282 (PI: Chu). For DEML71 and SNR 0548-70.4, the images were obtained with the F475W (B band), F555W (V band), F814W (I band), and F656N ($H\alpha$ line) filters. For SNR 0519-69.0, new images were obtained with only the F475W and F814W filters, because *HST* F550M and F658N images taken with the Advanced Camera for Sur-

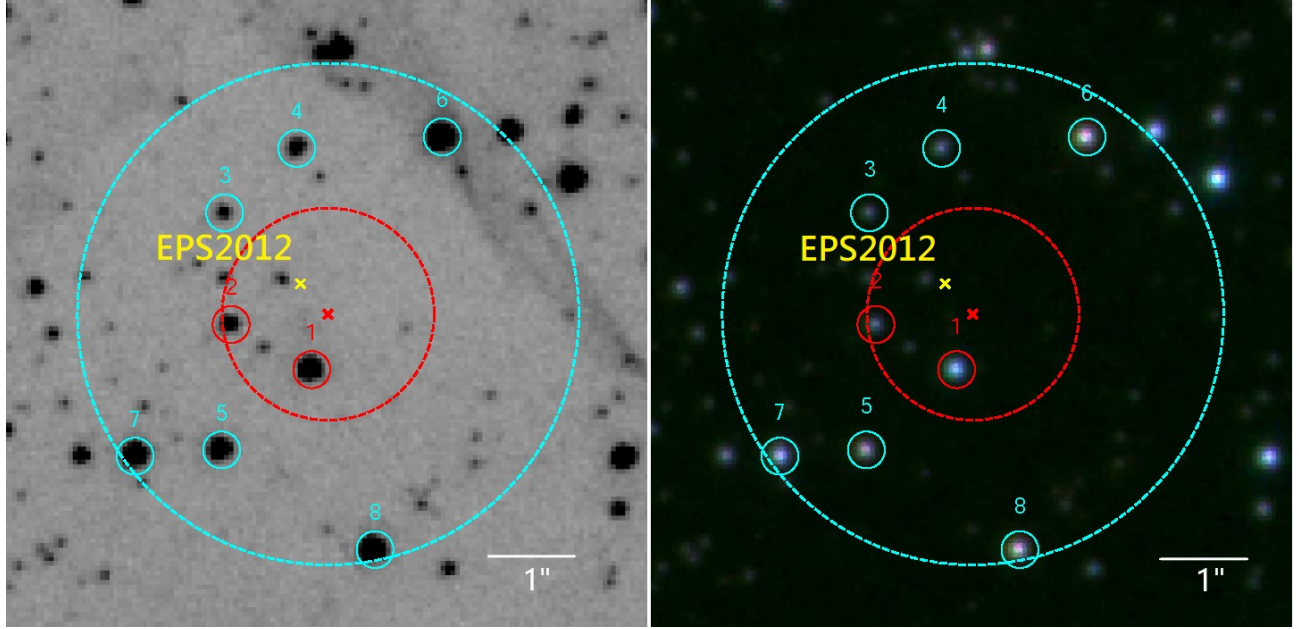


FIG. 5.— Left: $H\alpha$ image of SNR 0519–69.0. Right: color-composite image of SNR 0519–69, with the F475W image in blue, the F550M image in green, and F814W image in red. The red cross marks the adopted explosion center at $05^{\text{h}}19^{\text{m}}34^{\text{s}}.77$, $-69^{\circ}02'07''.25$ (J2000) in this work. The yellow cross marks the explosion center in [EPS2012](#). The stars with $V < 23$ within $2''.7$ from the center are marked and numbered in both the $H\alpha$ image and the color-composite image. The dashed red and cyan circles over the images illustrate our $1''.2$ (0.3 pc) and $2''.7$ (0.7 pc) runaway distances for the MS and helium star surviving companions.

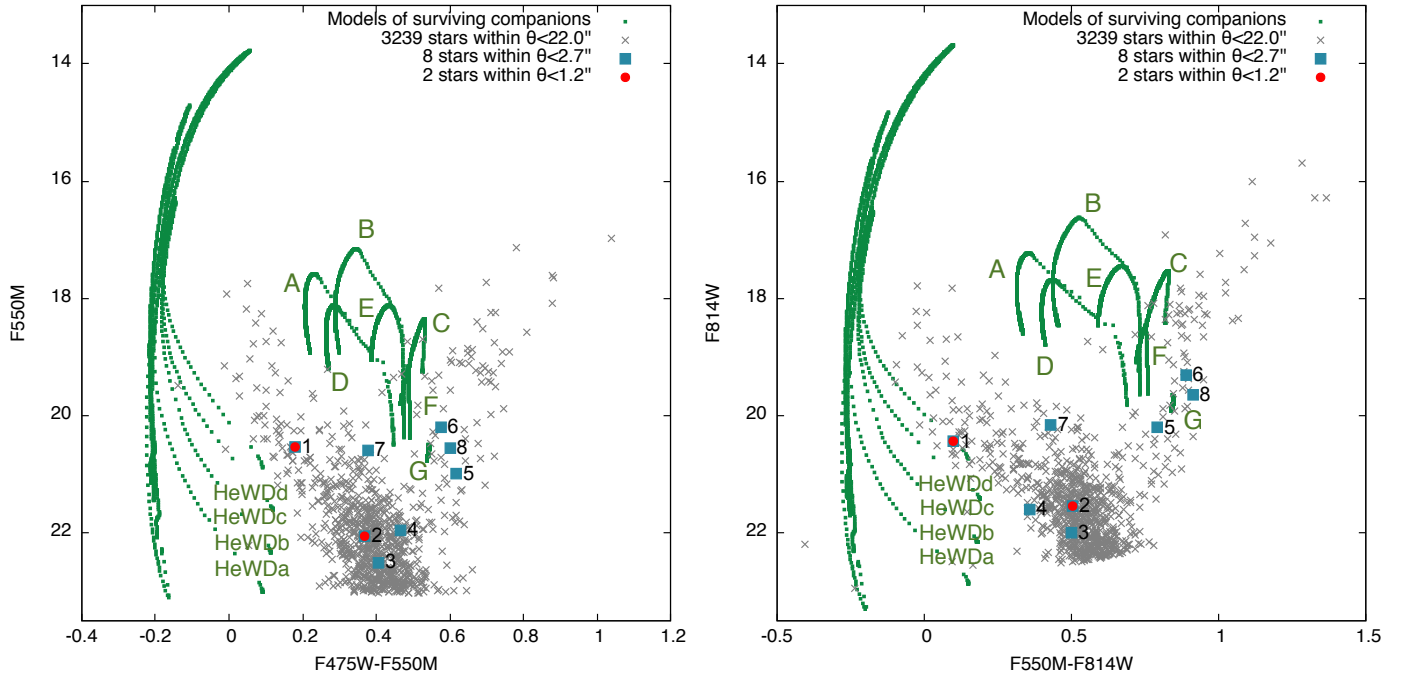


FIG. 6.— Left: The V versus $B - V$ CMD of stars projected in and near the SNR 0519–69.0. Right: The I versus $V - I$ CMD of the same stars. Stars that are found within the runaway distances of helium star and main-sequence (MS) surviving companions from the center are plotted in blue filled squares and red filled circles, respectively. Stars that are superposed on and near the remnant are plotted as gray crosses to illustrate the general background stellar population. The post-impact evolutionary tracks are plotted in small green squares, and those of surviving helium star and MS companions are to the left and above the MS, respectively. Different tracks of helium star and MS companions correspond to different companion mass in a range of 0.70 to 1.21 M_{\odot} and 1.17 to 1.88 M_{\odot} , respectively. The details of these helium star and MS companions can be found in models of [Pan et al. \(2014\)](#).

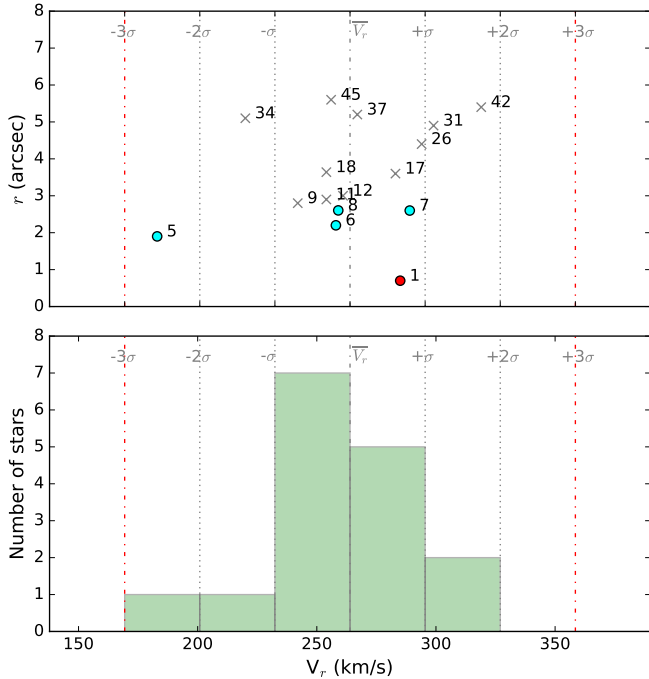


FIG. 7.— Top: a plot of the radial velocity (V_r) versus the distance to the site of SN explosion (r) for stars with $V < 21.6$ mag within a $6''.0$ radius in the SNR 0519–69.0. The stars within $1''.2$ and $2''.7$ from the site of explosion are marked as red and cyan solid circles, respectively. The background stars within $6''.0$ from the explosion site are marked as grey crosses. Bottom: the cumulative number of stars within standard deviations (σ) from the mean of radial velocity (\bar{V}_r).

veys (ACS) are available in the Hubble Legacy Archive. The *HST* images used in this paper are listed in Table 1. The continuum band images can be used to search for surviving companions and study the underlying stellar population, while the $H\alpha$ images can be used to analyze physical structures of the remnants and to determine their explosion centers.

The UVIS channel of WFC3 has a $162'' \times 162''$ field of view. The $0''.04$ pixel size corresponds to 0.01 pc in the LMC, at a distance of ~ 50 kpc. The observations of DEM L71 and SNR 0548–70.4 were dithered with the WFC3-UVIS-GAP-LINE pattern for 3 points and point spacings of $2''.414$. Each observation had a minimum total exposure time of 1050 s. In order to mitigate the charge transfer efficiency (CTE) issues in WFC3, FLASH = 5, 11 and 4 options were used for the F475W, F656N and F814W observations, respectively. The observations of SNR 0519–69.0 in the F475W and F814W passbands were dithered using POSTARG. The F475W observation had a total exposure time of 1070 s, and FLASH = 5; the F814W observation had a total exposure time of 1174 s, and FLASH = 4.

To examine the stars projected within or near the three Balmer-dominated SNRs, we have used the stellar photometry package DOLPHOT, adapted from HSTPHOT with *HST*-specific modules (Dolphin 2000), to perform point-spread function photometry on the *HST* images. Following Williams et al. (2014), we adopt specific criteria

on photometric parameters, such as signal-to-noise ratio ($S/N > 5$), $sharp^2 < 0.1$, and $crowd < 1.0$, to filter out non-stellar sources (Dolphin 2000). All stars have been measured in the Vega magnitude system for the B , V , and I passbands. The *HST* photometry allows us to compare the locations of stars in the CMDs with the expected evolutionary tracks of the post-impact surviving companions.

2.2. Chandra X-ray Observations

SNR 0519–69.0, DEM L71 and SNR 0548–70.4 were observed with the Advanced CCD Imaging Spectrometer (ACIS) of the *Chandra* X-ray Observatory for Program 01500024 (PI: Holt; 39.2 ks), Program 01500900 (PI: Hughes; 45.6 ks), and Program 02500872 (PI: Borkowski; 59.3 ks), respectively. The event files of these observations are available in the Chandra Data Archive, and images in various energy bands are conveniently available from the Chandra Supernova Remnant Catalog¹. While these SNRs are detected from 0.3 keV to 4–7 keV, the 0.3–2.1 keV band contains the bulk of the X-ray emission and the 0.3–2.1 keV band images are used to locate the boundaries of SNRs in order to assess their explosion centers.

2.3. VLT MUSE Observations

Multi-Unit Spectroscopic Explorer (MUSE) observations of SNR 0519–69.0 and DEM L71 were obtained with the Very Large Telescope (VLT) UT4 of the European Southern Observatory (ESO) on 2015 November 16 and 2016 January 17 (see Table 2) for Program 096.D-0352(A) (PI: Leibundgut). VLT MUSE is an integral-field Unit (IFU), providing optical spectrum for every position in the field of view (FOV). The wide-field mode used for the observations has a $60'' \times 60''$ FOV. This FOV is large enough to cover the entire SNR 0519–69.0 and adequate surroundings for background, but only about 80% of DEM L71 and a small region for background. The spectral coverage is 4750 – 9350 Å, which includes nebular emission lines such as $H\alpha$, $H\beta$, $[O III]\lambda\lambda 4595, 5007$, $[N II]\lambda\lambda 6548, 6583$, and $[S II]\lambda\lambda 6716, 6731$, as well as stellar absorption lines such as $H\alpha$, $H\beta$, He I $\lambda 5875$, He II $\lambda 5411$ and $\lambda 4686$, and Na I D-lines $\lambda\lambda 5890, 5896$. The spatial and spectral samplings are $0''.2$ spaxel⁻¹ and 1.25 Å pixel⁻¹, respectively. The VLT MUSE observations of SNR 0519–69.0 and DEM L71 each had an exposure time of 900 s.

We use the VLT MUSE data reduction pipeline (Weilbacher et al. 2014) to process bias subtraction, flat fielding, and wavelength and geometrical calibrations. The fields are crowded and large parts of the FOV are covered by either stars or nebular emission. To subtract the sky background, we use one pointing to blank sky and assume that the result would be viable for all pointings, and make use of algorithms from the Zurich Atmospheric Package (Soto et al. 2016); however, artificial flux fluctuations are found in the wavelength range 7700 – 9000 Å, and they are likely caused by the imperfect subtraction of sky background. To perform the flux calibration, we use existing photometry of stars in the field and synthetic photometry from the VLT MUSE data cube to make

¹ <https://hea-www.harvard.edu/ChandraSNR/index.html>

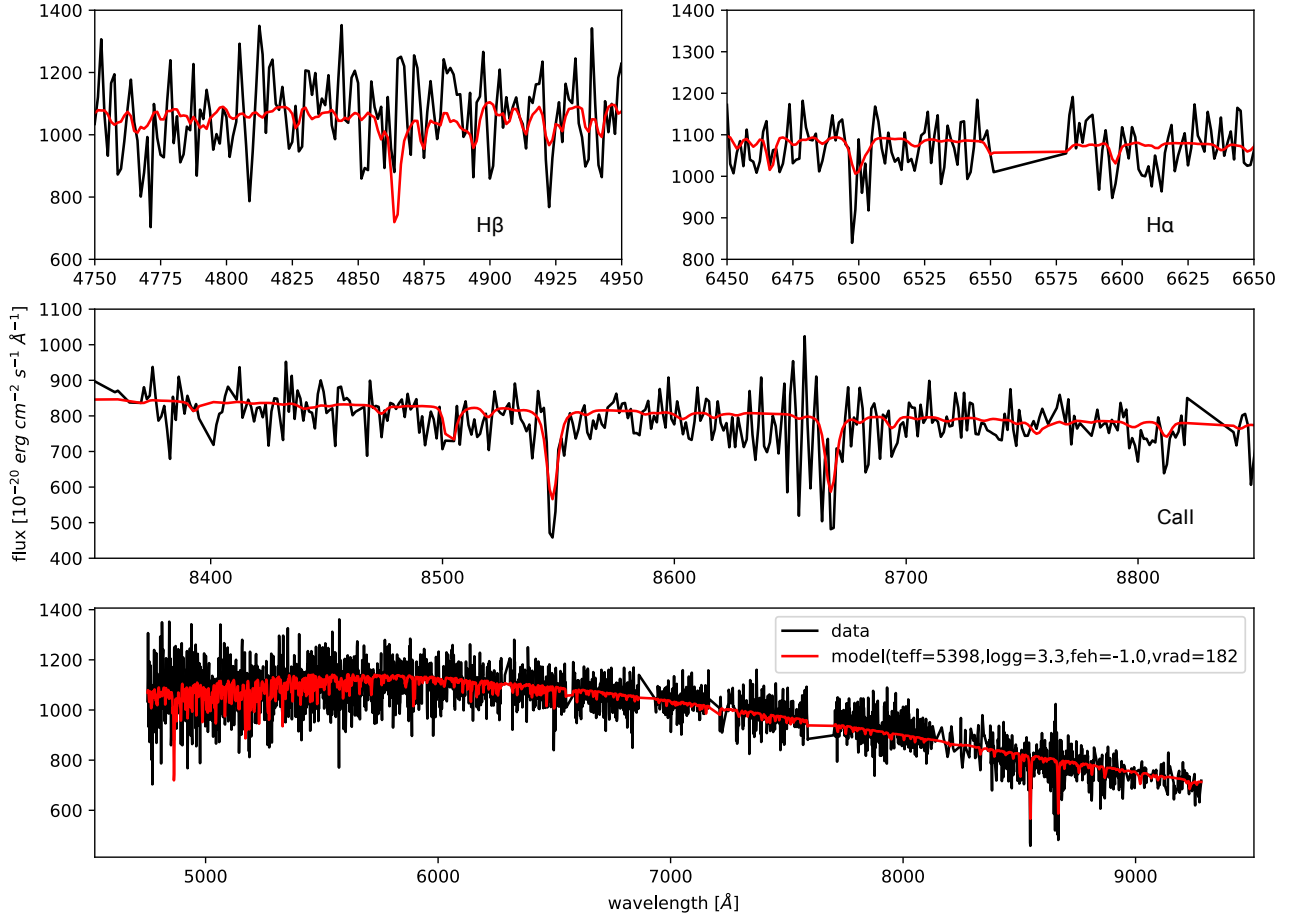


FIG. 8.— The VLT MUSE spectrum of star 5 in SNR 0519–69.0. Top: close-up wavelength windows around $H\beta$ and $H\alpha$ lines. Middle: close-up Ca II lines. Bottom: the stellar spectrum and its model fit. A systematic uncertainty term has been added in quadrature to statistical uncertainties of the fit, as shown in Table 5.

sure that differences of magnitudes of stars are within 0.05 mag. The detailed procedures of data reduction are described in Krühler et al. (2017). The VLT MUSE observations can be used to carry out spectroscopic analyses to search for stars that have large peculiar radial velocities.

2.3.1. Extracting Spectra from VLT MUSE Data

We use the **PampelMUSE** package (Kamann et al. 2013) to extract spectra of all stars with $V < 23.0$ mag within search radii from the centers of SNR 0519–69.0 and DEM L71. This software is well-designed with the purpose of improving the analysis of crowded stellar fields in IFU observations, and its graphical user interface (GUI) allows us to check the results visually in an interactive mode. To identify the sources that are feasible to extract the spectra, **PampelMUSE** requires an accurate reference catalogue which covers relative positions and magnitudes of the stars in the MUSE field of view. In this study, we use the high-resolution *HST* observations in contin-

uum bands as the reference. From the *HST* catalogue, **PampelMUSE** creates a mock image of stellar field from the existing photometry of stars. This mock image is used to cross-correlate with the VLT MUSE data in the routine **INITFIT**, to estimate positions of the sources that allow us to extract spectra in the VLT MUSE observations. From their positions, **INITFIT** identifies the sources as the resolved stars if they pass the criteria for the measured and modeled parameters, such as a local density of brighter sources < 0.4 per resolution element, a $S/N > 3$, and a distance to the nearest brighter source > 0.3 full width at half maximum (FWHM) of the point spread function (PSF).

Once the resolved stars in the VLT MUSE observations are identified, the routine **CUBEFIT** extracts all stellar spectra by fitting the PSF, the positions and the flux of these resolved stars layer by layer for the VLT MUSE data cube. In this step, we used the Moffat function to be the PSF profile, avoiding underestimation of the PSF wings for the Gaussian function. Afterwards, the routine

TABLE 3
EXPLOSION CENTERS AND SEARCH RADIUS

SNR (name)	Previous*			Center of ellipse		Adopted center		Search radius	
	R.A. (J2000)	Decl. (J2000)	R _{search} (arcsec)	R.A. (J2000)	Decl. (J2000)	R.A. (J2000)	Decl. (J2000)	R _{MS} (arcsec)	R _{helium} (arcsec)
0519–69.0	5:19:34.83	-69:02:06.92	4.7	5:19:34.72	-69:02:07.57	5:19:34.77	-69:02:07.25	1.2	2.7
DEM L71	5:05:42.71	-67:52:43.50	15.8	5:05:42.06	-67:52:41.00 ^a	5:05:42.04	-67:52:41.58	5.7	14.5
DEM L71	-	-	-	5:05:42.03	-67:52:42.17 ^b	-	-	-	-
0548–70.4	-	-	-	5:47:48.46	-70:24:52.43	5:47:48.46	-70:24:52.43	20.0	40.0

* The previous search of surviving companion in SNR 0519–69.0 and DEM L71 has been reported by [EPS2012](#) and [PS2015](#) respectively.

^{a, b} For DEM L71, we visually fit two ellipses to the shell with and without considering the blowout-like structures, respectively. We adopt the average of centers of the ellipses as the explosion center.

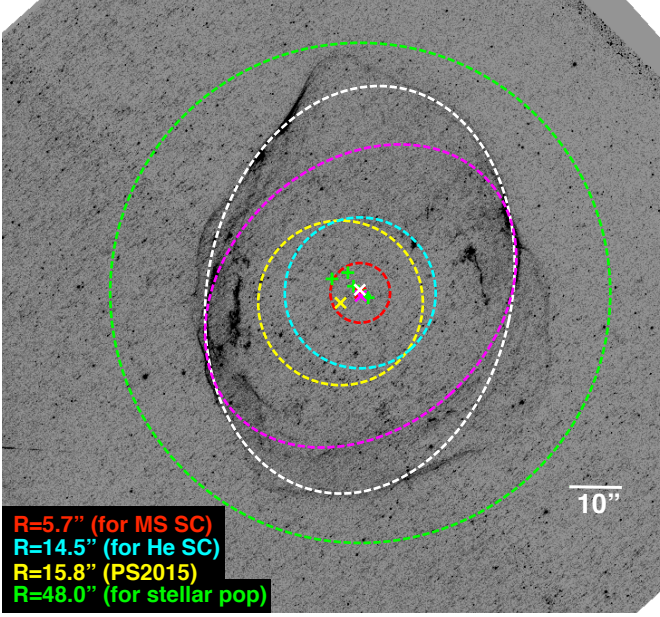


FIG. 9.— Same as Figure 4, but for DEM L71. We have visually fitted two ellipses (white and magenta) to the shell and mark their centers and their average for comparison. The detail is described in the Section 5.1.

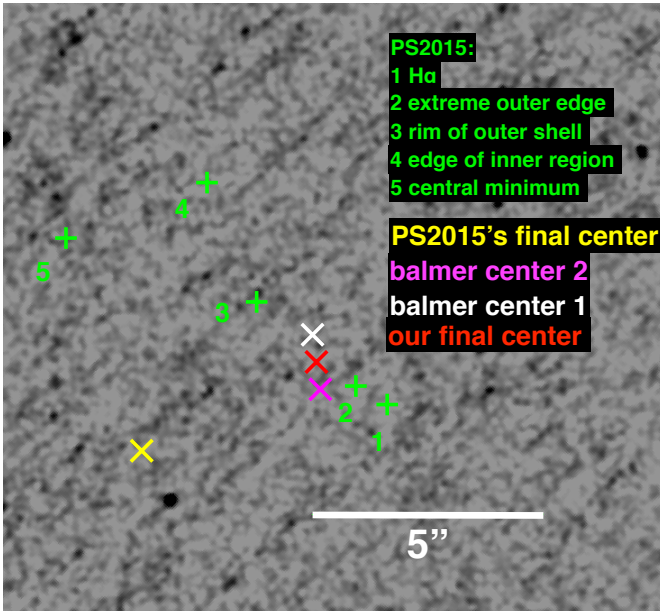


FIG. 10.— Close-up H α image of different centers of DEM L71.

POLYFIT fits the wavelength dependence of the PSF parameters and the VLT MUSE coordinates to smooth the fitted variations caused by the atmosphere refraction. In our analysis, the routine POLYFIT was performed with a fifth order Legendre polynomial. With these polynomial fits, we run the routine CUBEFIT again to extract the final spectra of the stars. In the end, we used the routine GETSPECTRA to save all stellar spectra into individual FITS file.

In the extracted stellar spectra, the presence of telluric lines would bias the spectral fits. To mitigate this problem, we identify the telluric absorption lines from the measurements of the VLT Ultraviolet and Visual Echelle Spectrograph (UVES) ([Dekker et al. 2000](#)), and manually remove the prominent telluric lines over the spectral coverage of 4750 – 9350 Å. Moreover, we find the Balmer absorption lines in some extracted stellar spectra are contaminated by Balmer line emission from nearby collisionless shocks. To make the spectral fits more reliable, we manually remove the contaminated Balmer emission lines, such as H β and H α lines, from those stellar spectra. The resulting spectra are used in the stellar spectra fitting to determine radial velocities.

2.3.2. Stellar Parameter Inference

Spectral template fitting with the PHOENIX grid was performed using the method described in [Do et al. \(2013\)](#) and [Støstad et al. \(2015\)](#) with the software package *StarKit* ([Kerzendorf & Do 2015](#)). *StarKit* is a modular spectral fitting framework using Bayesian inference to determine the best fit parameters and their uncertainties. *StarKit* simultaneously fits the physical parameters of stars, the spectral continuum, the radial velocity, and the rotational velocity. The set of physical parameters available for fitting is determined by the parameters sampled by the spectral grid. For the PHOENIX grid, the parameters are stellar effective temperature T_{eff} , surface gravity $\log g$, metallicity $[M/H]$, and α -element to iron abundance ratio $[\alpha/Fe]$. We use a linear interpolator to interpolate between the synthetic spectral grid points. We then convolve the spectral resolution of the grid to $R = 3,000$ in order to match the instrumental resolution.

Statistically, the fit is done by computing the posterior distribution in Bayes' Theorem:

$$P(\theta|D) = \frac{P(D|\theta)P(\theta)}{P(D)} \quad (1)$$

where D is the observed spectrum, and the model parameters $\theta = (T_{eff}, \log g, [M/H], [\alpha/Fe], V_r, V_{rot})$, where V_r

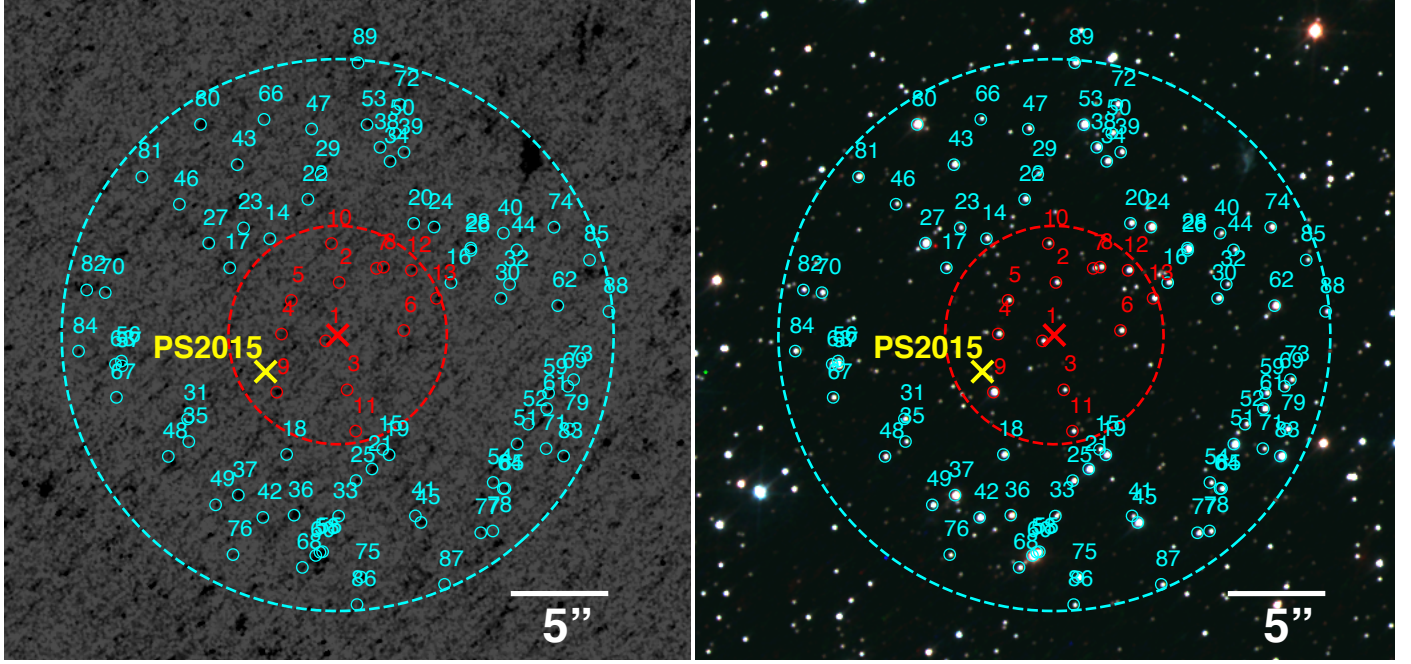


FIG. 11.— Same as Figure 5, but for DEM L71.

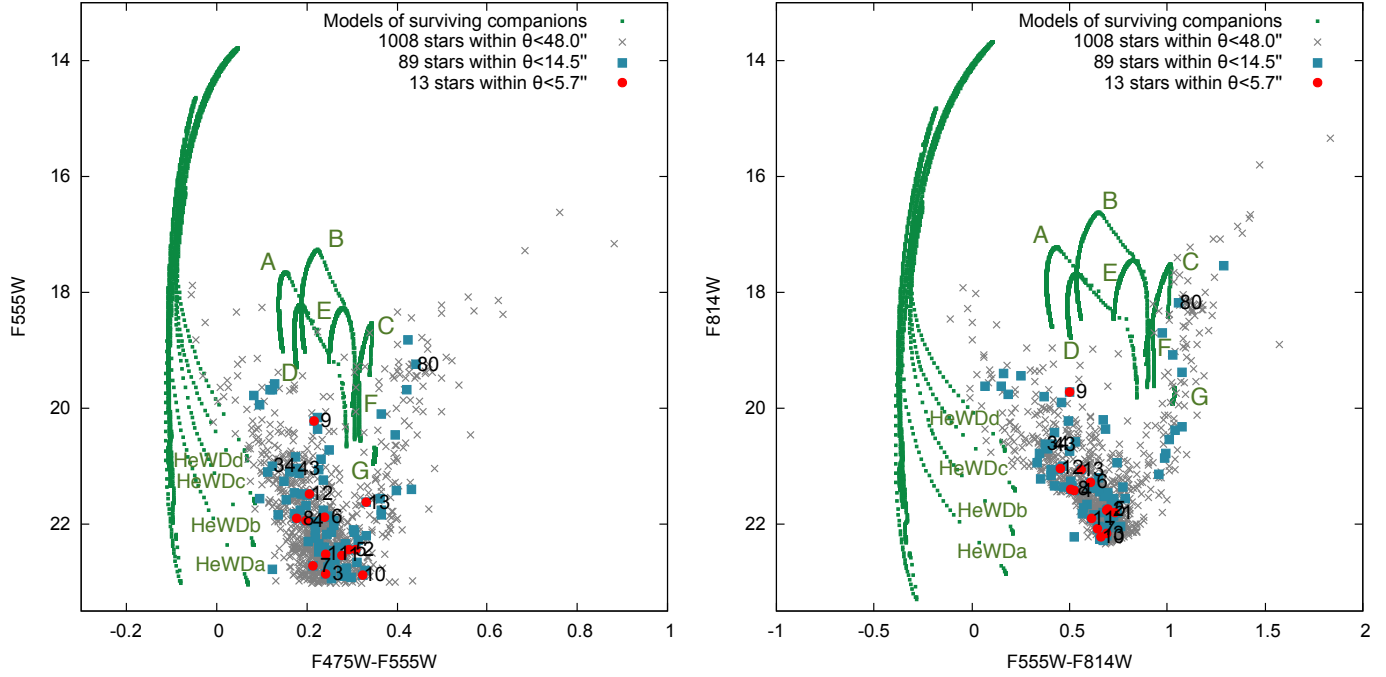


FIG. 12.— Same as Figure 6, but for DEM L71. Left: V versus $B - V$ CMD. Right: I versus $V - I$ CMD. The photometry of 89 candidates of MS surviving companions within $14''.5$ from the center of DEM L71 is summarized in Table 6.

is the radial velocity and V_{rot} is the rotational velocity. The priors on the model parameters are $P(\theta)$ and $P(D)$ is the evidence, which acts as the normalization. The combined likelihood for an observed spectrum is:

$$P(D|\theta) = \prod_{\lambda=\lambda_0}^{\lambda_n} \frac{1}{\epsilon_{\lambda,obs} \sqrt{2\pi}} \exp(-(F_{\lambda,obs} - F_{\lambda}(\theta))^2 / 2\epsilon_{\lambda,obs}^2), \quad (2)$$

where $F_{\lambda,obs}$ is the observed spectrum, $F_{\lambda}(\theta)$ is the model

spectrum evaluated with a given set of model parameters, and $\epsilon_{\lambda,obs}$ is the 1σ uncertainty for each observed flux point. This likelihood assumes that the uncertainty for each flux point is approximately Gaussian. For computational efficiency, we use the log-likelihood in place of the likelihood:

$$\ln P(D|\theta) \propto -\frac{1}{2} \sum_{\lambda=\lambda_0}^{\lambda_n} ((F_{\lambda,obs} - F_{\lambda}(\theta))^2 / \epsilon_{\lambda,obs}^2). \quad (3)$$

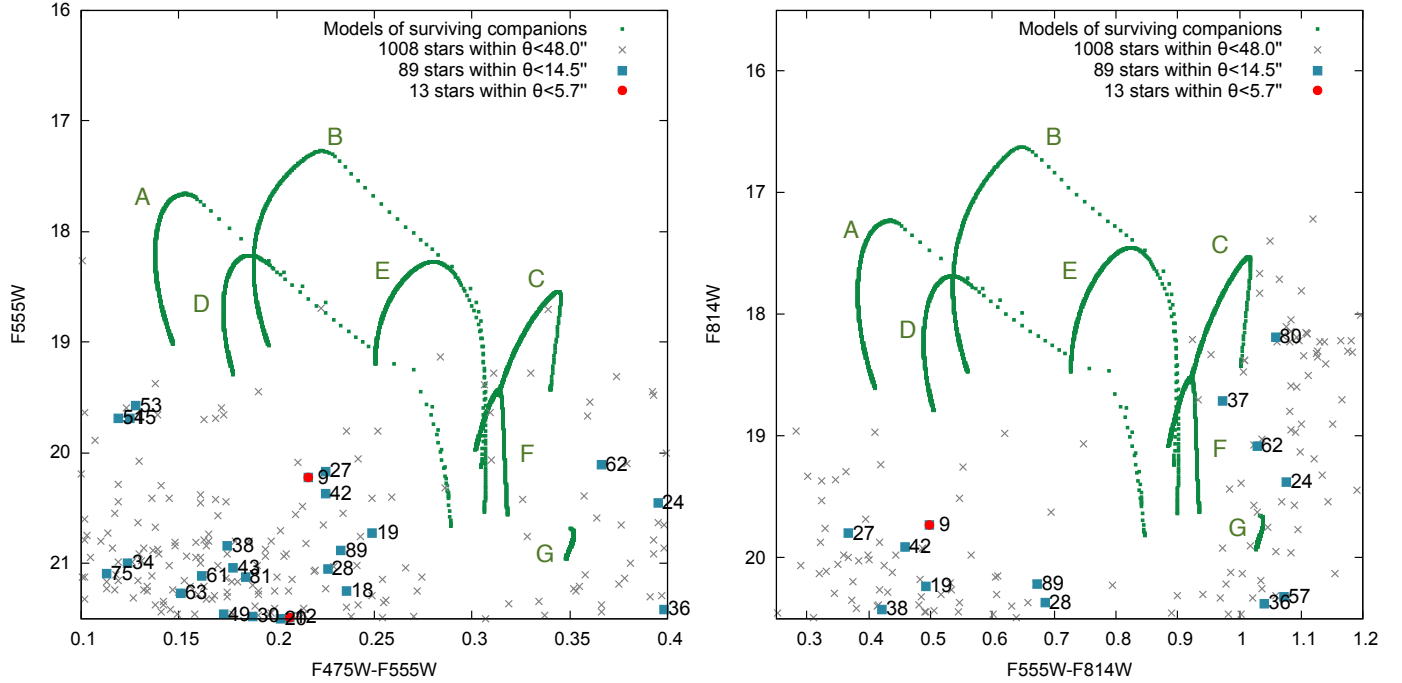


FIG. 13.— Close-up (Left) V versus B – V and (Right) I versus V – I CMDs near the evolutionary tracks for the case of surviving MS stars of DEML71.

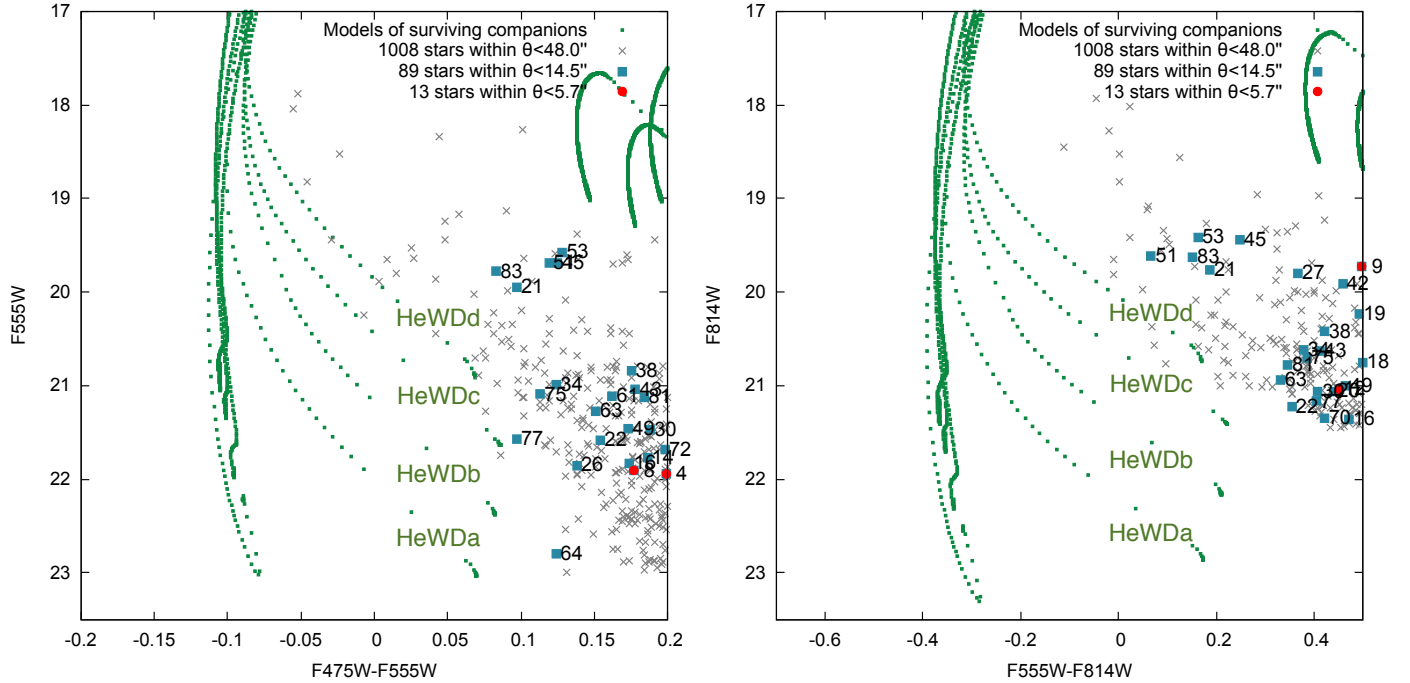


FIG. 14.— A close-up I versus V – I CMD near the evolutionary tracks for the case of surviving helium stars of DEML71.

We use flat priors in all the fit parameters and sample the posterior using Nestle, a nested sampling implementation (Feroz et al. 2009). We use the peak posterior value to be the best fit values and the marginalized 68% central confidence intervals for each fit parameter to be its uncertainty. Based on the tests against empirical references described in Feldmeier-Krause et al. (2017), we include a systematic uncertainty term added

in quadrature to the statistical uncertainties of each fit of $\sigma_{T_{eff}} = 200$ K, $\sigma_{[M/H]} = 0.2$, $\sigma_{[\alpha/Fe]} = 0.2$, and $\sigma_{\log g} = 1.0$.

3. METHODOLOGY

To search for the surviving companion of a Type Ia SN progenitor, we first locate the site of SN explosion, estimate possible range of velocity for a surviving com-

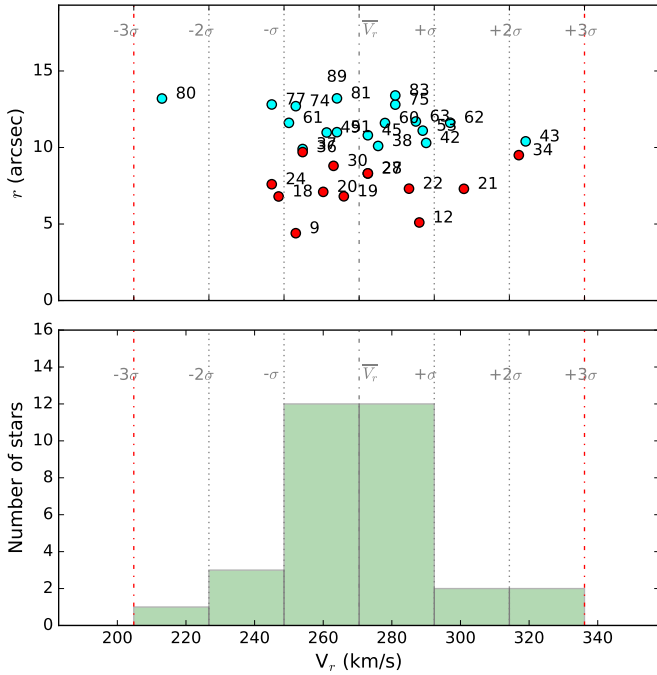


FIG. 15.— Top: a plot of radial velocity (V_r) versus the distance to the site of SN explosion (r) for stars with $V < 21.6$ mag within a $14''.5$ radius in DEM L71. The stars within $5''.7$ and $14''.5$ from the site of explosion are marked as red and cyan solid circles, respectively. Bottom: the cumulative number of stars within standard deviations (σ) from the mean of radial velocity (\bar{V}_r).

panion, and determine the search radius. We then use two methods to search for surviving companions within this radius. In the first method, we compare *HST* photometric measurements of stars with those expected from models of post-impact evolution of surviving companions (Pan et al. 2014). In the second method, we use MUSE observations to carry out spectroscopic analyses of stars and search for large peculiar radial velocities as diagnostics of surviving companions.

3.1. Site of SN Explosion and Search Radius

After the explosion of a Type Ia SN, the SN ejecta expands and interacts with the partially neutral ambient medium to produce the Balmer-dominated shell (Chevalier et al. 1980). If its progenitor had a non-degenerate stellar companion, as in the SD scenario, the stellar companion would survive the explosion and run away at a velocity comparable to its final orbital velocity. If the binary progenitor had a translational motion through the ISM (e.g., N103B, Li et al. 2017), the Balmer dominated shell would still be centered at the site of SN explosion as the expansion velocity of the SN ejecta is much higher than the progenitor’s translational velocity. The surviving companion will run away from the site of SN explosion at a velocity that is the sum of its orbital velocity and the progenitor’s translational velocity.

With the above understandings, we first estimate the site of SN explosion using the Balmer-dominated shell. If an SNR’s Balmer shell is regular and exhibits reflection symmetry about two orthogonal lines of symmetry,

the shell can be fitted by an ellipse, and its geometric center can be easily identified and measured with small uncertainties. We then adopt the geometric center to be the SN explosion site (e.g., Litke et al. 2017).

If an SNR’s Balmer shell is irregular, we still visually fit its general shape with an ellipse. Usually, over 75% of the shell periphery can be fitted well by an ellipse, and regions showing large deviations are faint and may be caused by a particularly low ambient density; thus, it is reasonable to adopt the center of the ellipse as the site of SN explosion. This is the case for SNR 0519–69.0 and SNR 0548–70.4.

If the ellipse fitted to an SNR’s Balmer shell is visibly unsatisfactory, for example, no ellipse can describe more than 70% of DEM L71’s Balmer shell periphery, then X-ray images of the reverse-shocked SN ejecta are used to make independent estimates of site of SN explosion (e.g., Schaefer et al. 2012, EPS2012, PS2015). The differences among these different estimates contribute to the uncertainty of the SN explosion site.

A surviving companion runs away from the site of SN explosion with a velocity that is the sum of its orbital velocity and the progenitor’s translational velocity. Assuming $\sim 2-3 M_\odot$ for a SN Ia progenitor’s total mass and a period of ≤ 1.0 day, the orbital velocity of the companion can reach as high as 400 km s^{-1} (Schaefer et al. 2012). The translational velocity of the SN progenitor is unknown, but it is most likely within the range of peculiar velocities of stars and much lower than velocities of runaway stars. In the post-impact models of surviving companion (Pan et al. 2014), the largest runaway velocity is 730 km s^{-1} for a helium star companion. To be on the safe side, we adopt a translational velocity of $< 100 \text{ km s}^{-1}$ and a “runaway velocity” of $< 730 \text{ km s}^{-1}$ for the surviving companion. Note that in a thermonuclear supernova model with a WD and a sub-dwarf helium star donor going through double detonation may eject the companion at velocities up to 900 km s^{-1} (Bauer et al. 2019; Geier et al. 2013); however, these surviving sub-dwarfs are too faint to be detected in the LMC.

The ages of the young Balmer-dominated SNRs have been determined from SN light echo observations (Rest et al. 2005) or sizes and shock velocities (Smith et al. 1991; Ghavamian et al. 2003). The “runaway distance” of a surviving companion from the site of SN explosion is equal to the runaway velocity times the SNR’s age t . We thus adopt a search radius of $7.5 \times 10^{-4} t_{\text{yr}}$ pc for the surviving companions. The younger the SNR is, the easier it is to search for a surviving companion within, as the surviving companion has not moved too far.

3.2. Photometric Search

The impact of SN ejecta on a non-degenerate stellar companion has been studied with numerous hydrodynamic simulations (Marietta et al. 2000; Pakmor et al. 2008; Pan et al. 2010, 2012; Liu et al. 2012, 2013; Bauer et al. 2019). Among these, Pan et al. (2014) have calculated the post-impact evolution of luminosity and effective temperature of the surviving companion and plotted them in the theoretical Hertzsprung-Russell (H-R) diagram, i.e., luminosity versus stellar effective temperature. For direct comparisons with observations, a blackbody model with the surviving companion’s temperature and luminosity is used to calculate its magnitudes in differ-

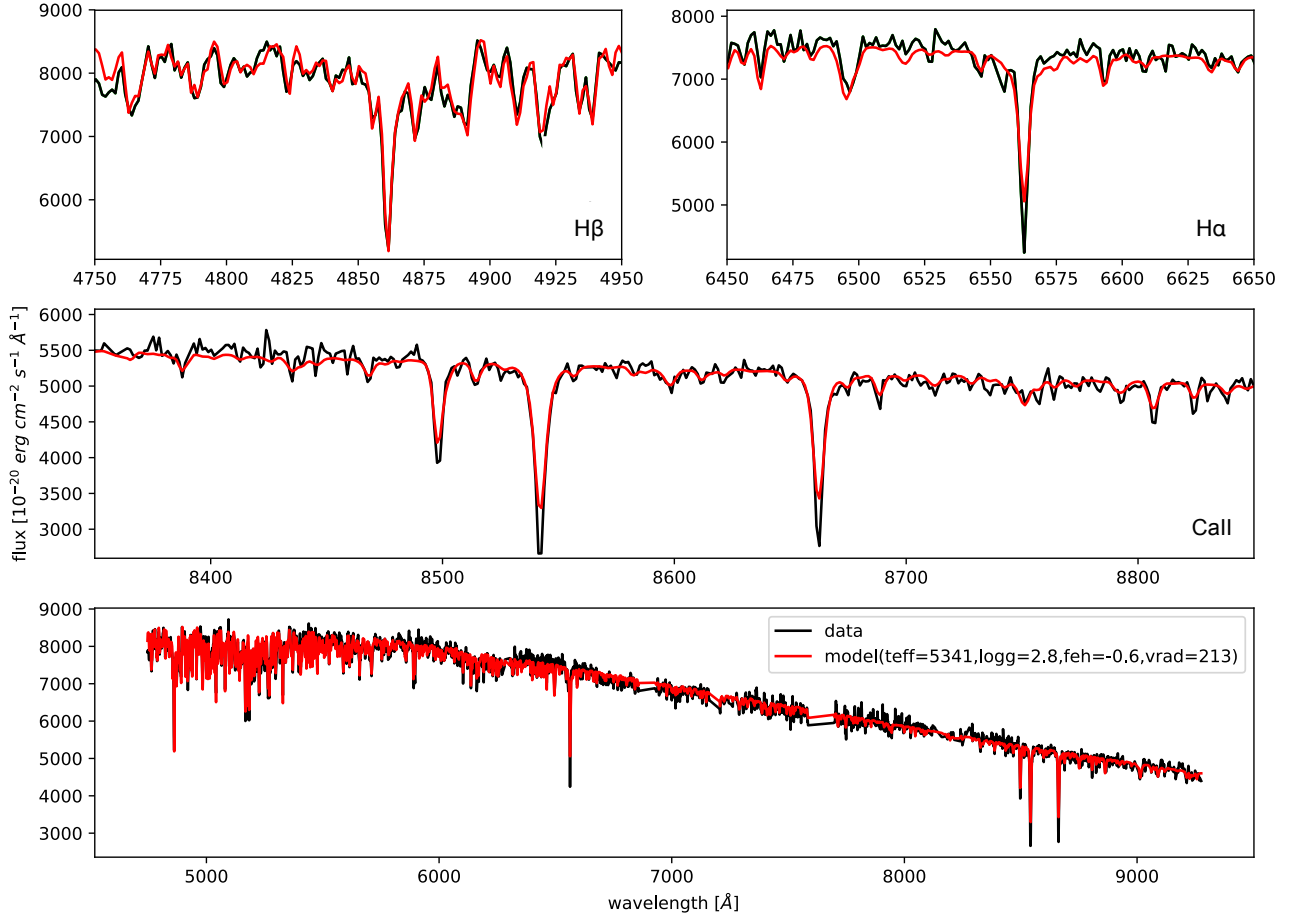


FIG. 16.— The VLT MUSE spectrum of star 80 in DEM L71. Top: close-up H β and H α lines. Middle: close-up Ca II lines. Bottom: the stellar spectrum and its model fit. A systematic uncertainty term has been added in quadrature to statistical uncertainties of the fit, as shown in Table 7.

ent passbands. The post-impact evolution of a surviving companion can then be plotted in an observational H-R diagram, i.e., color-magnitude diagrams (CMDs).

Schaefer et al. (2012) have considered various published SD models for Type Ia SN progenitors, such as recurrent novae, symbiotic stars, supersoft sources, helium donor companions, etc., and suggested that a surviving companion would have $V < 22.7$ mag at the distance of the LMC. Thus, in this study we consider only stars with $V < 23.0$ in the search for surviving companions.

We plot both stars in the search radius and stars within a large radius encompassing the entire SNR and some surrounding regions in V versus $B-V$ and I versus $V-I$ CMDs. Stars within the large radius allow us to establish a background stellar population for comparison. We then compare the stars in the search radius with the post-impact evolutionary tracks of surviving companions from Pan et al. (2012, 2013, 2014). A star falling on an evolutionary track with consistent age would be a candidate for surviving companion. Only few stars appear double

and too blended for reliable photometric measurements, and most of these are outside the search radii; therefore, we choose to ignore them.

3.3. Stars with Peculiar Radial Velocities

We use VLT MUSE observations of SNR 0519–69.0 and DEM L71 to carry out spectral analyses of stars within the search radius from the site of SN explosion, and use stellar atmosphere model fits to determine physical parameters and radial velocities of stars. We find that stellar atmosphere models show more reliable fits for stars with $V < 21.6$ mag. This turns out a safe limiting magnitude for our spectroscopic search for surviving MS companions, as the post-impact evolution of surviving MS companions modeled by Pan et al. (2014) show V well brighter than ~ 21.0 mag within the Balmer-dominated phase of Type Ia SNRs, less than $\sim 10,000$ yr after the SN blast. We thus spectroscopically examine the photometric candidates of surviving companions that have $V < 21.6$ and are located within the search radii, using large

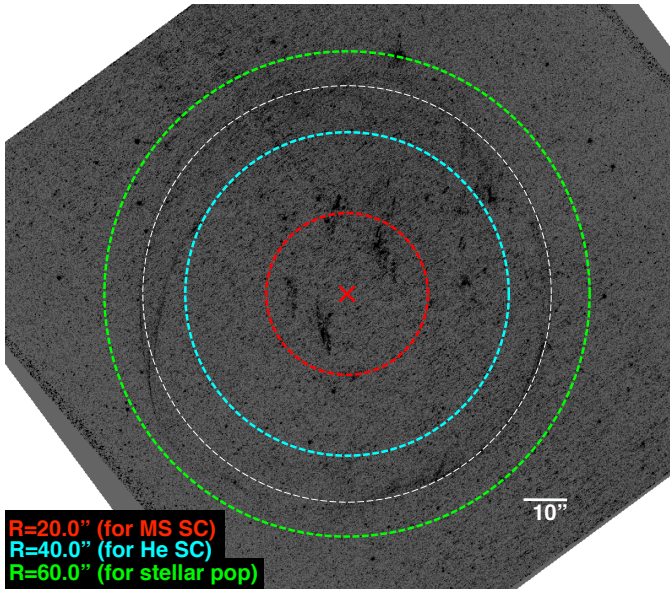


FIG. 17.— Same as Figure 9, but for SNR 0548–70.4.

radial velocities as diagnostics of surviving companions.

The distributions of radial velocities of these stars are plotted and examined. The standard deviation of the distribution, σ , is computed. Assuming a Gaussian distribution of the radial velocities, we expect only 0.3% of the population to have velocities deviating by more than 3σ from the mean (\bar{V}_r). For a population of <200 stars, fewer than 1 star is expected to be $>3\sigma$ from the mean. Therefore, stars with radial velocities more than 3σ from the mean are carefully examined to determine whether they are viable candidates for surviving companions of the SN progenitors.

4. INVESTIGATION OF SNR 0519–69.0

The previous search for surviving companion in SNR 0519–69.0 by EPS2012 used only *HST* V and $H\alpha$ band images. We have obtained additional B and I band images. This full set of data, in B , V , I , and $H\alpha$ bands, allow us to carry out more accurate analyses of the underlying stellar population.

4.1. Site of SN Explosion and Search Radius

EPS2012 argued that the SNR shell of 0519–69.0 does not suggest highly asymmetric explosion and that its geometric center is close to the site of SN explosion. They used 9 sets of perpendicular bisectors from edge to edge for the $H\alpha$ shell and X-ray shell, and adopted their average center, $05^{\text{h}}19^{\text{m}}34^{\text{s}}.83$, $-69^{\circ}02'06''.92$ (J2000), to be the site of SN explosion in SNR 0519–69.0. In our study, we fit an ellipse to the bright rim of the Balmer-dominated shell and adopt its center as the site of SN explosion, $05^{\text{h}}19^{\text{m}}34^{\text{s}}.72$, $-69^{\circ}02'07''.57$ (J2000). As shown in Figure 4, there is an offset of $0''.45$ between our center and that of EPS2012. This offset is caused by our different treatment of the faint northeast arc – we consider it an anomaly due to a lower density in this quadrant and ignore it when fitting an ellipse to the $H\alpha$ shell rim, while EPS2012 included the faint arcs as the shell edge. Without knowing details of the explosion geometry, we can only treat the difference in these two de-

terminations of SN explosion site as additional uncertainty. We adopt the average of centers determined by EPS2012 and our method as the site of SN explosion, $05^{\text{h}}19^{\text{m}}34^{\text{s}}.77$, $-69^{\circ}02'07''.25$ (J2000), see Figure 4. The coordinates of these centers are listed in Table 3.

SNR 0519–69.0 has an age of 600 ± 200 yrs (Rest et al. 2005). Adopting the largest runaway velocity of a surviving MS companion, 270 km s^{-1} , and a surviving helium star companion, 730 km s^{-1} (Pan et al. 2014), the runaway distance for a surviving MS companion can be up to 0.2 pc ($0''.9$), and a surviving helium star companion up to 0.6 pc ($2''.5$). The search radii for MS and helium star companions listed in Table 3 are determined by adding the uncertainty of explosion center, $0''.2$, to the runaway distance. All stars with $V < 23.0$ mag within the helium star search radius, $2''.7$, are examined for plausible candidates of surviving companion.

4.2. Photometric Search

Within the search radius $2''.7$ in SNR 0519–69.0, only eight stars are brighter than $V = 23.0$ mag. These eight stars, numbered in the order of increasing distance from the explosion center, are listed in Table 4 and marked in the close-up images in Figure 5 and the V versus $B-V$ and I versus $V-I$ CMDs in Figure 6. These stars are too few to show clearly the locations of the MS and the RG branch in the CMDs. We have thus plotted stars with $V < 23.0$ mag within $2''.0$ from the site of SN explosion in the CMDs in Figure 6. The greatest majority of these stars belong to the background stellar population, and the MS and RG branch are clearly visible in the CMDs, providing convenient references for candidate stars within the search radius.

In these CMDs we have also plotted the post-impact evolutionary tracks of MS (the curved tracks above the MS) and helium star (the vertical tracks to the left of the MS) surviving companions (Pan et al. 2014). None of the eight stars within $2''.7$ from the site of explosion fall on the two sets of tracks. Thus we conclude that no viable candidates of surviving MS or helium star companion are present based on the V versus $B-V$ and I versus $V-I$ CMDs, consistent with but more stringent than the conclusion of EPS2012.

4.3. Stars with Peculiar Radial Velocities

Only five stars are brighter than $V = 21.6$ mag within the search radius $2''.7$ of SNR 0519–69.0. The physical parameters and radial velocities of these stars are derived from model fits and are listed in Table 5. We have plotted the radial velocities of these five stars versus their distance to the SN explosion site in Figure 7. These five stars are too few to illustrate a statistically meaningful radial velocity distribution; therefore, we have added all stars with $V < 21.6$ mag within $6''.0$ from the SN explosion site in Figure 7 to show the radial velocity distribution in this neighborhood. It is noted that this larger radius, $6''.0$, encompasses candidate stars with $V < 21.6$ mag that are selected in EPS2012. From Figure 7, we find that star 5 has a radial velocity, $182 \pm 0 \text{ km s}^{-1}$, that deviates more than 2.5σ from the mean velocity, 264 km s^{-1} ; furthermore, its radial velocity is not well populated by the LMC or Galactic stars. To examine whether the radial velocity from model fit is reliable, we display

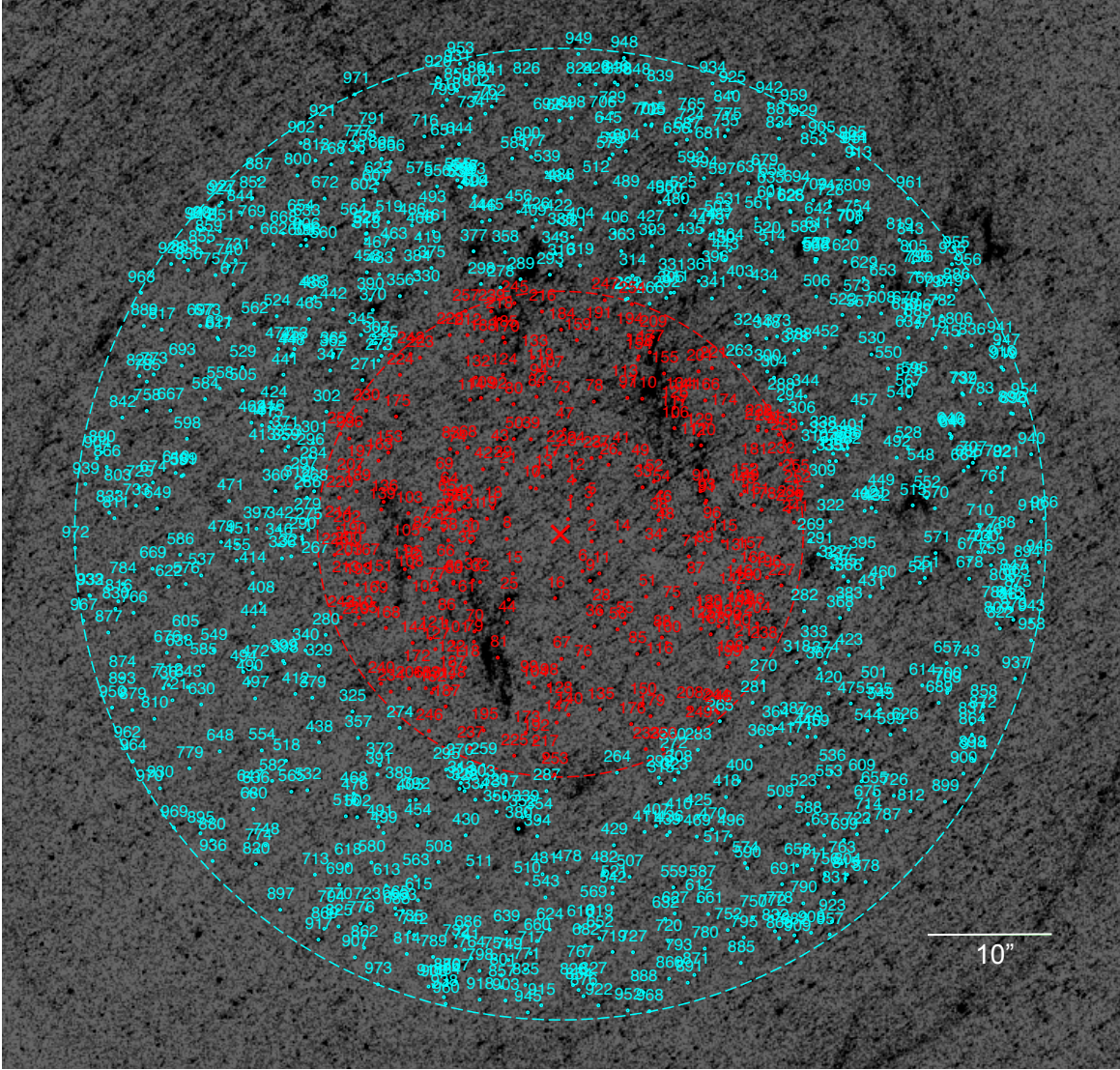


FIG. 18.— Same as the left panel in Figure 5, but for SNR 0548–70.4.

TABLE 4
STARS BRIGHTER THAN $V = 23.0$ MAG NEAR CENTRAL REGION IN THE SNR 0519–69.0

Star	R.A. (J2000)	Decl. (J2000)	B	V	I	B-V	V-I	r
1	05:19:34.81	-69:02:7.85	20.72 ± 0.00	20.54 ± 0.00	20.44 ± 0.01	0.18 ± 0.00	0.10 ± 0.01	$0.63''$
2	05:19:34.97	-69:02:7.36	22.42 ± 0.01	22.05 ± 0.01	21.54 ± 0.01	0.37 ± 0.01	0.50 ± 0.01	$1.06''$
3	05:19:34.98	-69:02:6.15	22.91 ± 0.01	22.50 ± 0.01	22.00 ± 0.01	0.41 ± 0.01	0.50 ± 0.01	$1.57''$
4	05:19:34.84	-69:02:5.45	22.42 ± 0.01	21.95 ± 0.01	21.60 ± 0.01	0.47 ± 0.01	0.36 ± 0.01	$1.83''$
5	05:19:34.99	-69:02:8.72	21.61 ± 0.01	21.00 ± 0.01	20.20 ± 0.01	0.62 ± 0.01	0.79 ± 0.01	$1.87''$
6	05:19:34.54	-69:02:5.33	20.77 ± 0.00	20.19 ± 0.00	19.30 ± 0.00	0.57 ± 0.00	0.89 ± 0.00	$2.29''$
7	05:19:35.16	-69:02:8.79	20.97 ± 0.00	20.59 ± 0.01	20.16 ± 0.01	0.38 ± 0.01	0.43 ± 0.01	$2.60''$
8	05:19:34.68	-69:02:9.80	21.15 ± 0.01	20.55 ± 0.00	19.64 ± 0.00	0.60 ± 0.01	0.91 ± 0.00	$2.60''$

the spectrum of star 5 with its model fit in Figure 8. As shown in this figure, the $H\alpha$ and $H\beta$ lines of star 5 are contaminated by the nearby Balmer-dominated shocks and are not possible for the determination of radial velocity, but the calcium line 8542.1\AA , with the model fit looks viable. This peculiar radial velocity indicates that star 5 may be a promising candidate of surviving companion. Furthermore, assuming that star 5 has a mass of $\sim 1 M_{\odot}$, the stellar effective temperature and surface gravity from the spectral fit implies an M_V of 2.54 mag, and the observed $V = 21.0$ mag requires the distance to

be ~ 49 kpc, consistent with the LMC distance. We will further discuss this star in Section 7.

5. INVESTIGATION OF DEM L71

The previous search for surviving companion in DEM L71 by PS2015 used Gemini GMOS g' , r' , i' , and $H\alpha$ images. We have obtained *HST* B , V , I , and $H\alpha$ images of DEM L71. These new *HST* images and VLT MUSE observations are used in our investigation.

5.1. Site of SN Explosion and Search Radius

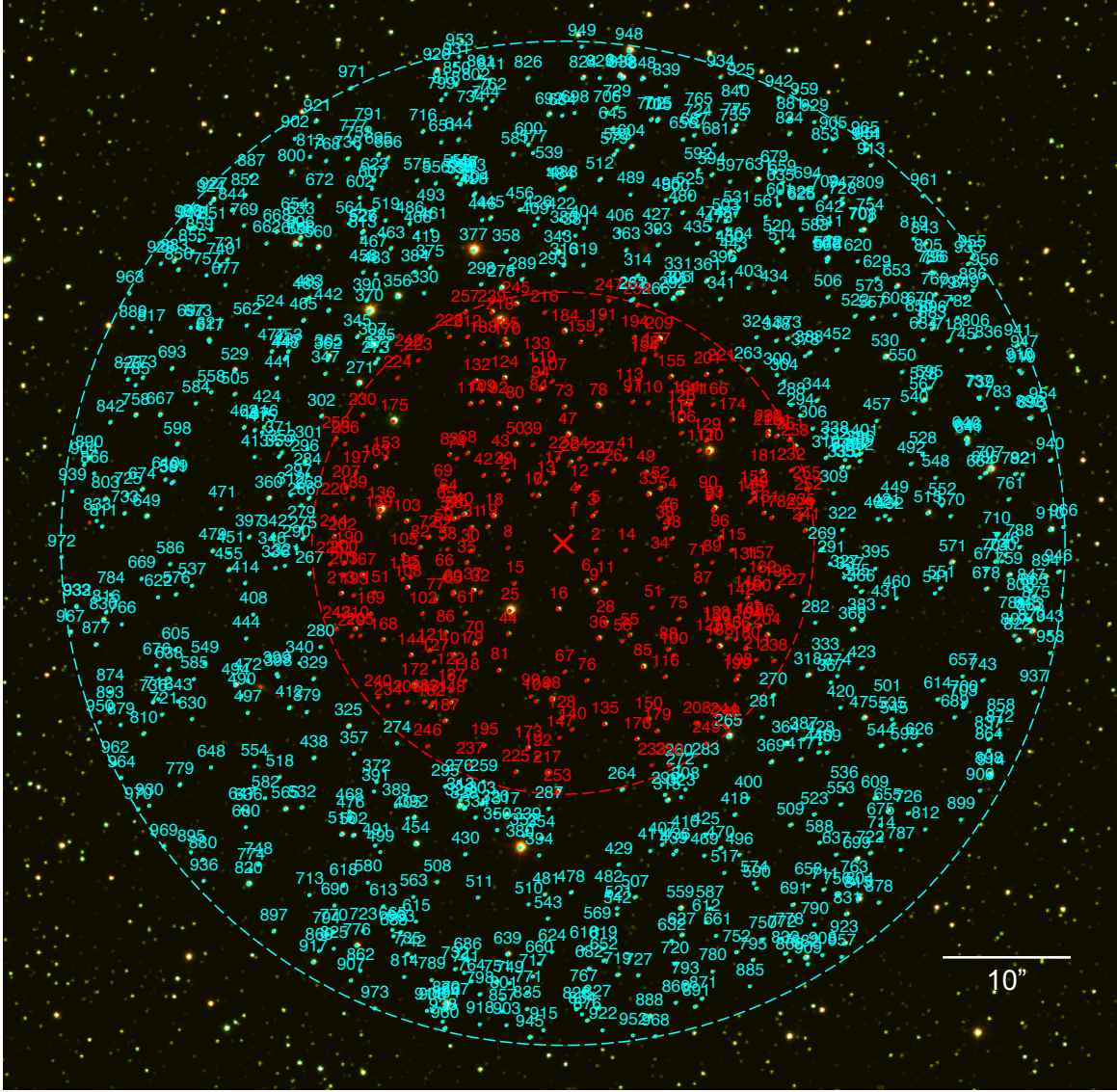


FIG. 19.— Same as the right panel in Figure 5, but for SNR 0548–70.4.

TABLE 5
STELLAR PARAMETERS OF THE STARS BRIGHTER THAN $V = 21.6$
MAG IN TABLE 4

Star	T_{eff} (K)	$\log g$ (dex)	[Fe/H] (dex)	V_r (km s $^{-1}$)
1	7873 ± 201	4.6 ± 1.0	-0.5 ± 0.2	285 ± 0
5	5398 ± 201	3.3 ± 1.0	-1.0 ± 0.2	182 ± 0
6	5263 ± 200	3.6 ± 1.0	-1.0 ± 0.2	258 ± 0
7	7000 ± 200	4.2 ± 1.0	-0.4 ± 0.2	289 ± 0
8	5042 ± 200	3.3 ± 1.0	-0.9 ± 0.2	259 ± 0

We have included a systematic uncertainty term added in quadrature to statistical uncertainties of each fit, based on the tests against empirical references described in [Feldmeier-Krause et al. \(2017\)](#). The details about the spectral fitting can be found in Section 2.3.2.

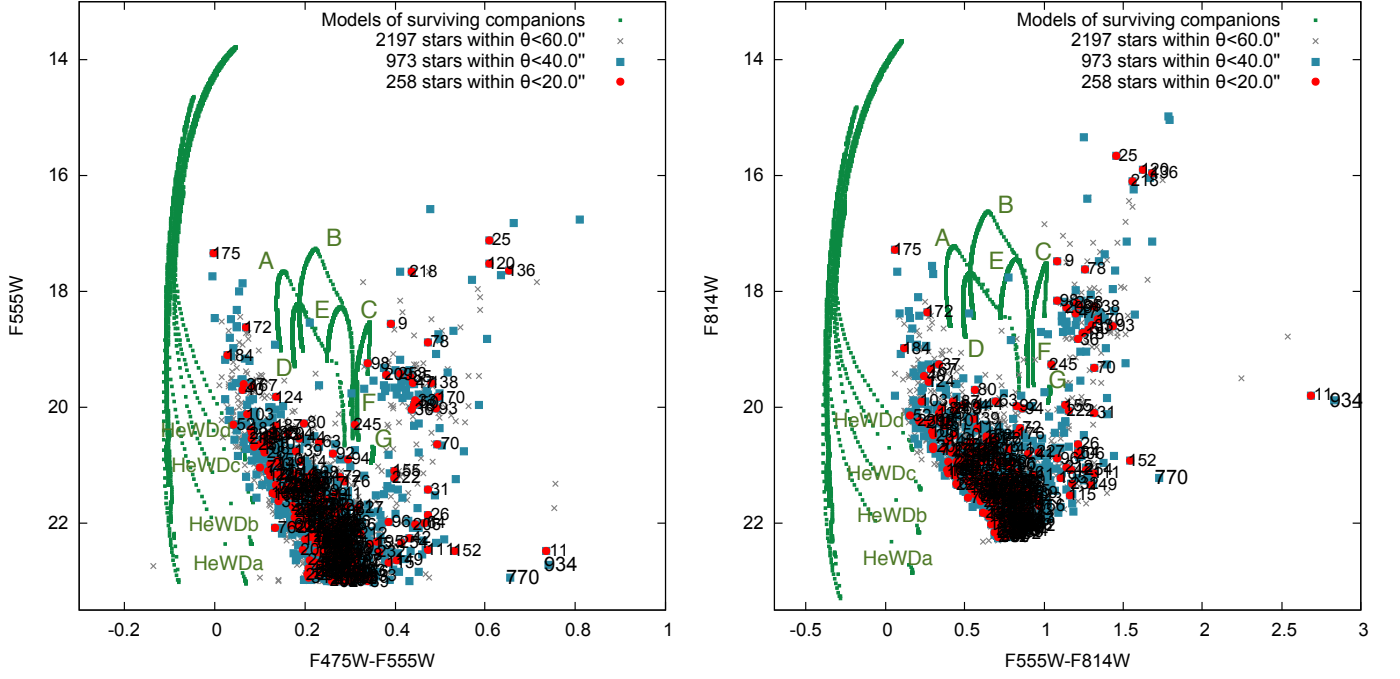


FIG. 20.— Same as Figure 6, but for SNR 0548–70.4. (Left) V versus B – V CMD (Right) I versus V – I CMD for the underlying stars of SNR0548–70.4.

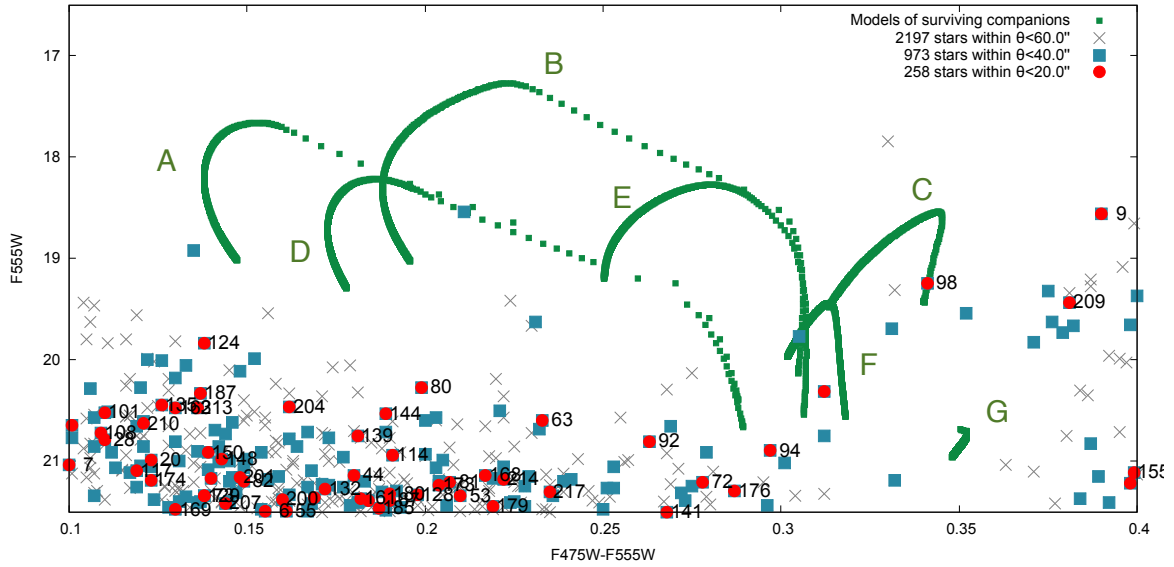


FIG. 21.— Close-up V versus B – V CMD for the case of MS stars of SNR 0548–70.4 .

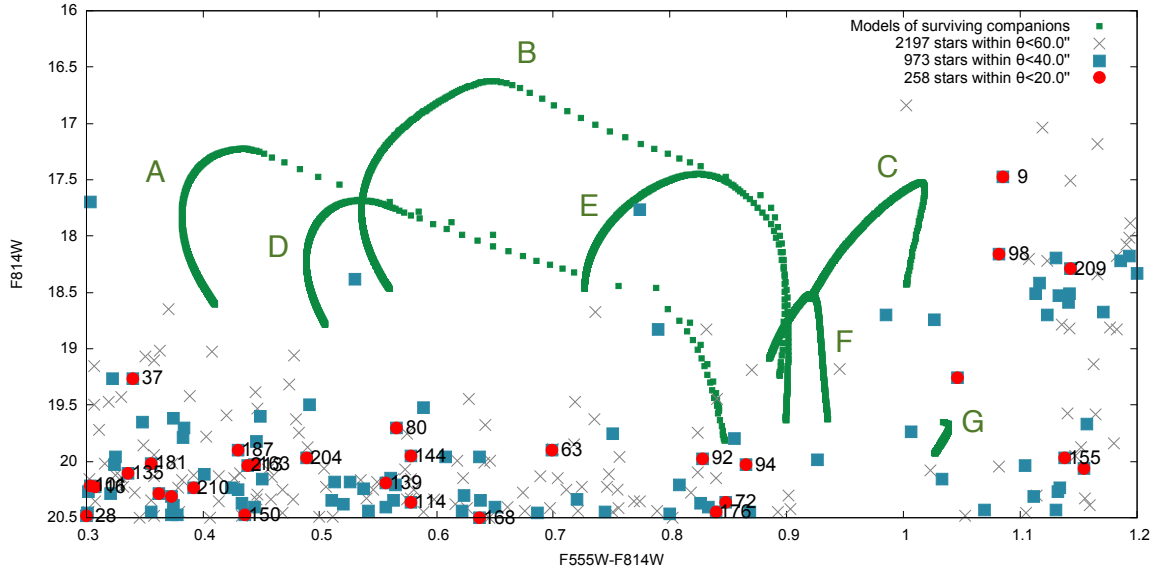


FIG. 22.— Close-up I versus V – I CMD for the case of MS stars of SNR 0548–70.4 .

PS2015 applied the perpendicular bisector method (Schaefer et al. 2012) to the GMOS H α image and *Chandra* X-ray images (Hughes et al. 2003; Rakowski et al. 2003) of DEM L71 to assess an average geometric center of the remnant, and adopted this center as the explosion site. For the X-ray images, the authors used four gas regions to locate the X-ray geometric center: the extreme faint outer edge, the bright rim of the outer shell, the inner region, and the central minimum. Their final SN explosion site is adopted to be 05^h05^m42^s.71, –67°52′43″50 (J2000). These centers are marked in Figure 10.

The physical origins of the above four gas regions are different and need to be noted. DEM L71 presents an ideal example of the double-shock structure, with forward shocks expanding into the ISM and reverse shocks moving into and heating the ejecta (Hughes et al. 2003; Rakowski et al. 2003). The outer shell in X-rays is thus associated with the forward (collisionless) shock into the partially neutral ISM. The bright X-ray shell rims correspond to sightlines parallel to the shock fronts and include the longest emitting path lengths, while the faint emission extending beyond the bright shell rim is associated with blowout-like structures into a lower-density medium. The inner X-ray emission region corresponds to SN ejecta that has been heated by the reverse shock, and the central minimum originates from the central cavity.

In our previous study of N103B (Li et al. 2017), the geometric center of its Balmer-dominated shell was identified as the site of SN explosion because the Balmer shell follows closely the shock fronts into the ISM. The Balmer-dominated shell of DEM L71 is somewhat irregular. We have visually fitted two ellipses to the shell (as shown in Figure 9) and mark their centers and their average in Figure 10 for comparison. Our centers are offset to the northeast of the H α center of PS2015 because of our different treatment of the faint southwest protrusion of the Balmer shell. We assume the faint protrusion is caused by a local anomalously low density in the ISM and fit ellipses to only the bright rims of the Balmer shell, while PS2015 include the outer edge of the protrusion in their derivation of H α center.

Figure 10 also shows that the centers PS2015 determined from the central minimum and the inner X-ray emission are both offset significantly to the northeast of the center we derived from the Balmer shell. As noted above, the inner X-ray emission is associated with the SN ejecta. This offset is expected because the SN ejecta carried the same orbital velocity of the WD while the Balmer shell interacts and expands in the ISM. The offset between the center of ejecta and the center of SNR is expected to increase with age.

The detailed analysis of physical structure of DEM L71 will be reported in a future paper. Here we adopt our average Balmer center as the site of SN explosion and use the difference between our centers as uncertainty. All centers are listed in Table 3.

DEM L71 has an age of 4360 ± 290 yr (Ghavamian et al. 2003). Adopting the largest runaway velocity, 270 km s^{-1} and 730 km s^{-1} , for surviving MS and helium star companions, respectively, the runaway distance for a surviving MS companion can be up to 1.3 pc ($5''.1$), and a surviving helium star companion up to 3.5 pc ($13''.9$). We determine the search radii for surviving MS and helium star companions by adding the uncertainty of the SN explosion site, $0''.6$, to the runaway distance. These search radii are listed in Table 3. In this study, all stars with $V < 23.0$ mag within the helium star search radius, $14''.5$, are examined as potential candidates of surviving companion.

5.2. Photometric Search

A total of 89 stars are brighter than $V = 23.0$ mag within the search radius $14''.5$ in DEM L71. These 89 stars are numbered in the order of increasing distance to the site of explosion and marked in the close-up images (Figure 11) and V versus $B-V$ and I versus $V-I$ CMDs (Figure 12). Their photometric measurements are listed in Table 6. In the CMDs, these 89 stars do not show clearly the locations of the MS and RG branch. We have thus plotted all stars with $V < 23.0$ mag within $48''.0$ from the site of explosion in the CMDs (Figure 12) in a different symbol (grey cross) to illustrate the MS and

RG branch in the CMDs.

In the CMDs (Figure 12), we have over-plotted the post-impact evolutionary tracks of the MS (the curved tracks above the MS) and helium star (the vertical tracks to the left of the MS) surviving companions (Pan et al. 2014). From locations of stars in the CMDs, we find no star matches the evolutionary tracks for MS and helium star surviving companion candidates within the search radius of $14''.5$, as shown in the close-up in Figure 13 and Figure 14. Our study has different search area and candidates from PS2015, but our photometric search has not found any obvious candidate of surviving companion, neither.

5.3. Stars with Peculiar Radial Velocities

There are 32 stars with $V < 21.6$ mag within the $14''.5$ search radius in DEM L71. The stellar parameters and radial velocities of these stars from model fits are listed in Table 7. We have plotted the distribution of radial velocities versus distances to the explosion site of these stars in Figure 15. While the overall distribution roughly reveals a Gaussian profile, we find that star 80 has a radial velocity, 213 ± 0 km s $^{-1}$, that are deviated more than 2.5σ from the mean, 270 km s $^{-1}$ (Figure 15); furthermore, its radial velocity is not well populated by the LMC or Galactic stars. The model fit of the spectrum of star 80, displayed in Figure 16, looks reasonable. The peculiar radial velocity of star 80 makes it an intriguing candidate for surviving companion. Assuming that star 80 has a mass of $\sim 1 M_{\odot}$, the stellar effective temperature and surface gravity from the spectral fit implies an M_V of 1.33 mag, and the star would be at a distance of ~ 38 kpc as it has an observed $V = 19.25$ mag; if a mass of $\sim 1.69 M_{\odot}$ is assumed, the star would be at a distance of ~ 50 kpc. Follow-up spectroscopic observations of star 80 in blue wavelengths are needed for better determination of its physical properties. We will further discuss this star in Section 7.

6. INVESTIGATION OF SNR 0548–70.4

No search for surviving companion in the SNR 0548–70.4 has been reported in the literature. In this study, we use our *HST* B , V , I , and $H\alpha$ images of SNR 0548–70.4 to analyze the underlying stellar population, and search for the surviving companion candidates. Unfortunately, no VLT MUSE observation of SNR 0548–70.4 is available for radial velocity analyses.

6.1. Site of SN Explosion and Search Radius

The Balmer shell of SNR 0548–70.4 shows a regular shape, similar to the case of SNR 0509–67.5 (Litke et al. 2017). We find that over 75% of the outer shell periphery can be well fitted by an ellipse. In the northwest and southeast quadrants, the faint extended emission deviates from the fitted ellipse, and appears to be associated with blowout structures. Thus we identify the center of the ellipse as the site of SN explosion. We will use a larger search radius to take into account the uncertainty due to the irregularity in the Balmer shell periphery.

We choose the MS and helium star search radii of SNR 0548–70.4 that are sufficiently larger than the respective runaway distances of the MS and helium star companions from the explosion site. SNR 0548–70.4 has an

age of 10,000 yr (Hendrick et al. 2003). Adopting the largest runaway velocity of 270 km s $^{-1}$ and 730 km s $^{-1}$ for surviving MS and helium star companions, we calculate their runaway distance up to 2.8 pc ($11''.0$) and 7.5 pc ($29''.8$), respectively. We then adopt 5.0 pc ($20''.0$) and 10.0 pc ($40''.0$) as the search radii for MS and helium star companions, respectively. These limits correspond to a kick velocity of 500 km s $^{-1}$ and 1000 km s $^{-1}$, respectively. All stars with $V < 23.0$ mag within the search radius of helium star, $40''.0$, are compiled for surviving companion candidates.

6.2. Photometric Search

Within the search radius $40''.0$ in SNR 0548–70.4, 973 stars are brighter than $V < 23.0$ mag. These 973 stars are numbered in the order of increasing distance from the explosion site and listed in Table 9 with their photometric measurements. We have marked these stars in the $H\alpha$ (Figure 18) and color-composite images (Figure 19), as well as in the V versus $B-V$ and I versus $V-I$ CMDs (Figure 20). In the CMDs, these stars show hints of the MS and the RG branch. To better illustrate the locations of the MS and RG branch in the CMDs, we have also plotted all stars with $V < 23.0$ mag within $60''.0$ from the explosion site.

In the CMDs (Figure 20), we have over-plotted the post-impact evolutionary tracks of surviving MS (the tracks above the MS) and helium star (the vertical tracks to the left of the MS) companions (Pan et al. 2014). We find that star 98 lies on a track of a surviving MS star model in the V versus $B-V$ CMD (Figure 21), but not in the I versus $V-I$ CMD (Figure 22); furthermore, its location in the V versus $B-V$ CMD indicates a MS surviving companion going through ~ 110 years after the SN explosion. It is not consistent with the age of SNR 0548–70.4, 10,000 yr (Hendrick et al. 2003). Assuming negligible extinction, star 98's $B - V \sim 0.34$ suggests an early F spectral type, and its $V - I \sim 1.08$ suggests an early K spectral type.

While photometric comparisons with post-impact evolution models in CMDs do not yield promising candidates for surviving companions, we notice puzzling photometric properties of star 11. In the CMDs, star 11 is located in regions not well populated by LMC or Galactic stars, as shown in Figure 20. It is far away from the post-impact evolution tracks of stars; furthermore, its colors are inconsistent with any spectral types. Assuming negligible extinction, star 11's $B - V \sim 0.74$ suggests a spectral type of G type and its $V - I \sim 2.68$ suggests a spectral type of M3 type. In the V band, star 11 is twice as bright as the Sun, while in the I band star 11 is 13 times as bright as the Sun. This particularly red $V - I$ color suggests infrared excess. Interestingly, star 770 and 934 appear puzzling photometric properties in the CMDs as well. These three stars will be discussed further in Section 7.

7. DISCUSSIONS

To differentiate between the SD and DD origins of a Type Ia SN, we use the strategy to search for a surviving companion within its SNR. (Marietta et al. 2000; Canal et al. 2001; Ruiz-Lapuente et al. 2004; González Hernández et al. 2009, 2012; Kerzendorf et al. 2014; Pan et al. 2014).

TABLE 6
STARS BRIGHTER THAN $V = 23.0$ MAG NEAR CENTRAL REGION IN THE
DEML71

Star	R.A. (J2000)	Decl. (J2000)	B	V	I	B-V	V-I	r
1	05:05:42.15	-67:52:41.89	22.82 \pm 0.01	22.54 \pm 0.01	21.80 \pm 0.01	0.28 \pm 0.01	0.73 \pm 0.01	0.70''
2	05:05:42.03	-67:52:38.82	22.75 \pm 0.01	22.44 \pm 0.01	21.75 \pm 0.01	0.31 \pm 0.01	0.69 \pm 0.01	2.76''
3	05:05:41.95	-67:52:44.45	23.10 \pm 0.01	22.86 \pm 0.01	22.17 \pm 0.01	0.24 \pm 0.01	0.69 \pm 0.01	2.92''
4	05:05:42.56	-67:52:41.53	22.14 \pm 0.01	21.95 \pm 0.01	21.42 \pm 0.01	0.20 \pm 0.01	0.52 \pm 0.01	2.95''
5	05:05:42.47	-67:52:39.76	22.73 \pm 0.01	22.44 \pm 0.01	21.75 \pm 0.01	0.29 \pm 0.01	0.69 \pm 0.01	3.04''
6	05:05:41.43	-67:52:41.34	22.12 \pm 0.01	21.88 \pm 0.01	21.27 \pm 0.01	0.24 \pm 0.01	0.60 \pm 0.01	3.47''
7	05:05:41.68	-67:52:38.08	22.94 \pm 0.01	22.73 \pm 0.01	22.08 \pm 0.01	0.21 \pm 0.01	0.64 \pm 0.01	4.04''
8	05:05:41.62	-67:52:38.02	22.09 \pm 0.01	21.91 \pm 0.01	21.40 \pm 0.01	0.18 \pm 0.01	0.51 \pm 0.01	4.29''
9	05:05:42.61	-67:52:44.58	20.44 \pm 0.00	20.22 \pm 0.00	19.73 \pm 0.00	0.22 \pm 0.00	0.50 \pm 0.00	4.39''
10	05:05:42.10	-67:52:36.78	23.21 \pm 0.01	22.88 \pm 0.01	22.22 \pm 0.01	0.32 \pm 0.01	0.66 \pm 0.01	4.81''
11	05:05:41.87	-67:52:46.62	22.76 \pm 0.01	22.52 \pm 0.01	21.91 \pm 0.01	0.24 \pm 0.01	0.61 \pm 0.01	5.13''
12	05:05:41.36	-67:52:38.18	21.69 \pm 0.01	21.49 \pm 0.01	21.04 \pm 0.01	0.21 \pm 0.01	0.45 \pm 0.01	5.14''
13	05:05:41.12	-67:52:39.65	21.96 \pm 0.01	21.63 \pm 0.01	21.07 \pm 0.01	0.33 \pm 0.01	0.56 \pm 0.01	5.52''
14	05:05:42.67	-67:52:36.52	21.96 \pm 0.01	21.77 \pm 0.01	21.27 \pm 0.01	0.19 \pm 0.01	0.50 \pm 0.01	6.19''
15	05:05:41.62	-67:52:47.57	22.60 \pm 0.01	22.28 \pm 0.01	21.56 \pm 0.01	0.31 \pm 0.01	0.72 \pm 0.01	6.44''
16	05:05:40.99	-67:52:38.83	22.00 \pm 0.01	21.82 \pm 0.01	21.35 \pm 0.01	0.17 \pm 0.01	0.47 \pm 0.01	6.54''
17	05:05:43.04	-67:52:38.05	22.10 \pm 0.01	21.85 \pm 0.01	21.21 \pm 0.01	0.25 \pm 0.01	0.65 \pm 0.01	6.68''
18	05:05:42.51	-67:52:47.85	21.48 \pm 0.01	21.25 \pm 0.01	20.75 \pm 0.01	0.24 \pm 0.01	0.50 \pm 0.01	6.82''
19	05:05:41.56	-67:52:47.86	20.97 \pm 0.01	20.72 \pm 0.00	20.23 \pm 0.01	0.25 \pm 0.01	0.49 \pm 0.01	6.84''
20	05:05:41.33	-67:52:35.72	21.70 \pm 0.01	21.50 \pm 0.01	21.06 \pm 0.01	0.20 \pm 0.01	0.44 \pm 0.01	7.09''
21	05:05:41.72	-67:52:48.61	20.04 \pm 0.00	19.95 \pm 0.00	19.76 \pm 0.00	0.10 \pm 0.00	0.19 \pm 0.00	7.25''
22	05:05:42.32	-67:52:34.46	21.73 \pm 0.01	21.58 \pm 0.01	21.23 \pm 0.01	0.15 \pm 0.01	0.35 \pm 0.01	7.29''
23	05:05:42.92	-67:52:35.96	22.89 \pm 0.01	22.63 \pm 0.01	21.93 \pm 0.02	0.26 \pm 0.01	0.70 \pm 0.02	7.49''
24	05:05:41.15	-67:52:35.91	20.85 \pm 0.01	20.45 \pm 0.00	19.38 \pm 0.00	0.40 \pm 0.01	1.08 \pm 0.00	7.59''
25	05:05:41.87	-67:52:49.22	22.21 \pm 0.01	21.84 \pm 0.01	20.86 \pm 0.01	0.37 \pm 0.01	0.98 \pm 0.01	7.70''
26	05:05:40.80	-67:52:37.14	21.99 \pm 0.01	21.85 \pm 0.01	21.34 \pm 0.01	0.14 \pm 0.01	0.51 \pm 0.01	8.28''
27	05:05:43.24	-67:52:36.76	20.39 \pm 0.00	20.17 \pm 0.00	19.80 \pm 0.00	0.23 \pm 0.00	0.37 \pm 0.00	8.31''
28	05:05:40.81	-67:52:37.01	21.28 \pm 0.01	21.05 \pm 0.00	20.37 \pm 0.01	0.23 \pm 0.01	0.69 \pm 0.01	8.34''
29	05:05:42.20	-67:52:33.15	22.80 \pm 0.01	22.54 \pm 0.01	21.80 \pm 0.01	0.26 \pm 0.01	0.74 \pm 0.01	8.48''
30	05:05:40.52	-67:52:39.66	21.66 \pm 0.01	21.48 \pm 0.01	21.07 \pm 0.01	0.19 \pm 0.01	0.41 \pm 0.01	8.77''
31	05:05:43.43	-67:52:45.98	22.62 \pm 0.01	22.34 \pm 0.01	21.55 \pm 0.01	0.28 \pm 0.01	0.78 \pm 0.01	9.02''
32	05:05:40.44	-67:52:38.91	23.11 \pm 0.01	22.85 \pm 0.01	22.19 \pm 0.01	0.26 \pm 0.01	0.67 \pm 0.01	9.40''
33	05:05:42.03	-67:52:51.08	23.06 \pm 0.01	22.81 \pm 0.01	22.07 \pm 0.01	0.25 \pm 0.01	0.75 \pm 0.01	9.50''
34	05:05:41.55	-67:52:32.47	21.12 \pm 0.01	20.99 \pm 0.01	20.62 \pm 0.01	0.12 \pm 0.01	0.38 \pm 0.01	9.52''
35	05:05:43.42	-67:52:47.17	23.05 \pm 0.01	22.77 \pm 0.01	22.11 \pm 0.01	0.28 \pm 0.01	0.66 \pm 0.01	9.61''
36	05:05:42.45	-67:52:51.03	21.81 \pm 0.01	21.41 \pm 0.01	20.37 \pm 0.01	0.40 \pm 0.01	1.04 \pm 0.01	9.73''
37	05:05:42.96	-67:52:49.98	20.11 \pm 0.00	19.68 \pm 0.00	18.71 \pm 0.00	0.42 \pm 0.00	0.97 \pm 0.00	9.89''
38	05:05:41.65	-67:52:31.73	21.02 \pm 0.01	20.84 \pm 0.00	20.42 \pm 0.01	0.17 \pm 0.01	0.42 \pm 0.01	10.10''
39	05:05:41.43	-67:52:31.98	22.41 \pm 0.01	22.11 \pm 0.01	21.15 \pm 0.01	0.30 \pm 0.01	0.96 \pm 0.01	10.20''
40	05:05:40.50	-67:52:36.23	23.14 \pm 0.01	22.86 \pm 0.01	22.19 \pm 0.01	0.28 \pm 0.01	0.67 \pm 0.01	10.20''
41	05:05:41.32	-67:52:51.07	23.20 \pm 0.01	22.95 \pm 0.01	22.28 \pm 0.01	0.26 \pm 0.01	0.67 \pm 0.01	10.33''
42	05:05:42.74	-67:52:51.15	20.59 \pm 0.00	20.37 \pm 0.00	19.91 \pm 0.01	0.23 \pm 0.00	0.46 \pm 0.01	10.34''
43	05:05:42.97	-67:52:32.64	21.22 \pm 0.01	21.04 \pm 0.00	20.63 \pm 0.01	0.18 \pm 0.01	0.41 \pm 0.01	10.38''
44	05:05:40.38	-67:52:37.11	22.95 \pm 0.01	22.70 \pm 0.01	22.05 \pm 0.01	0.25 \pm 0.01	0.65 \pm 0.01	10.41''
45	05:05:41.27	-67:52:51.41	19.81 \pm 0.00	19.69 \pm 0.00	19.44 \pm 0.00	0.13 \pm 0.00	0.25 \pm 0.00	10.76''
46	05:05:43.51	-67:52:34.72	23.10 \pm 0.01	22.85 \pm 0.01	22.18 \pm 0.01	0.25 \pm 0.01	0.67 \pm 0.01	10.78''
47	05:05:42.28	-67:52:30.77	22.79 \pm 0.01	22.54 \pm 0.01	21.80 \pm 0.01	0.25 \pm 0.01	0.74 \pm 0.01	10.90''
48	05:05:43.61	-67:52:47.95	22.21 \pm 0.01	21.95 \pm 0.01	21.34 \pm 0.01	0.26 \pm 0.01	0.60 \pm 0.01	10.94''
49	05:05:43.17	-67:52:50.49	21.64 \pm 0.01	21.46 \pm 0.01	21.00 \pm 0.01	0.17 \pm 0.01	0.47 \pm 0.01	10.98''
50	05:05:41.51	-67:52:31.00	22.32 \pm 0.01	22.10 \pm 0.01	21.44 \pm 0.01	0.22 \pm 0.01	0.66 \pm 0.01	11.00''
51	05:05:40.37	-67:52:47.30	19.80 \pm 0.00	19.68 \pm 0.00	19.62 \pm 0.00	0.12 \pm 0.00	0.07 \pm 0.00	11.01''
52	05:05:40.27	-67:52:46.25	22.67 \pm 0.01	22.40 \pm 0.01	21.66 \pm 0.01	0.27 \pm 0.01	0.74 \pm 0.01	11.04''
53	05:05:41.77	-67:52:30.54	19.70 \pm 0.00	19.57 \pm 0.00	19.41 \pm 0.00	0.13 \pm 0.00	0.16 \pm 0.00	11.14''
54	05:05:40.60	-67:52:49.31	22.84 \pm 0.01	22.58 \pm 0.01	21.86 \pm 0.01	0.25 \pm 0.01	0.73 \pm 0.01	11.24''
55	05:05:42.18	-67:52:52.95	22.46 \pm 0.01	22.24 \pm 0.01	21.66 \pm 0.01	0.22 \pm 0.01	0.59 \pm 0.01	11.40''
56	05:05:44.05	-67:52:42.95	22.45 \pm 0.01	22.14 \pm 0.01	21.37 \pm 0.01	0.31 \pm 0.01	0.77 \pm 0.01	11.43''
57	05:05:44.04	-67:52:43.20	21.83 \pm 0.01	21.39 \pm 0.01	20.32 \pm 0.01	0.43 \pm 0.01	1.07 \pm 0.01	11.44''
58	05:05:42.21	-67:52:52.98	22.13 \pm 0.01	21.76 \pm 0.01	20.77 \pm 0.01	0.36 \pm 0.01	0.99 \pm 0.01	11.44''
59	05:05:40.08	-67:52:44.62	22.41 \pm 0.01	22.15 \pm 0.01	21.46 \pm 0.01	0.26 \pm 0.01	0.69 \pm 0.01	11.47''
60	05:05:42.24	-67:52:53.14	19.25 \pm 0.00	18.82 \pm 0.00	17.54 \pm 0.00	0.42 \pm 0.00	1.29 \pm 0.00	11.62''
61	05:05:40.10	-67:52:45.44	21.27 \pm 0.01	21.11 \pm 0.01	20.58 \pm 0.01	0.16 \pm 0.01	0.53 \pm 0.01	11.63''
62	05:05:40.00	-67:52:40.04	20.48 \pm 0.00	20.11 \pm 0.00	19.08 \pm 0.00	0.37 \pm 0.00	1.03 \pm 0.00	11.64''
63	05:05:44.10	-67:52:43.11	21.42 \pm 0.01	21.27 \pm 0.01	20.94 \pm 0.01	0.15 \pm 0.01	0.33 \pm 0.01	11.76''
64	05:05:40.50	-67:52:49.64	22.91 \pm 0.01	22.79 \pm 0.01	22.10 \pm 0.01	0.12 \pm 0.01	0.69 \pm 0.01	11.85''
65	05:05:40.49	-67:52:49.62	22.97 \pm 0.01	22.66 \pm 0.01	21.94 \pm 0.01	0.31 \pm 0.01	0.72 \pm 0.01	11.90''
66	05:05:42.72	-67:52:30.26	23.00 \pm 0.01	22.75 \pm 0.01	22.23 \pm 0.01	0.25 \pm 0.01	0.52 \pm 0.01	11.96''
67	05:05:44.10	-67:52:44.85	22.54 \pm 0.01	22.21 \pm 0.01	21.53 \pm 0.01	0.33 \pm 0.01	0.68 \pm 0.01	12.07''
68	05:05:42.37	-67:52:53.77	22.43 \pm 0.01	22.19 \pm 0.01	21.51 \pm 0.01	0.24 \pm 0.01	0.68 \pm 0.01	12.33''
69	05:05:39.90	-67:52:44.27	22.57 \pm 0.01	22.34 \pm 0.01	21.62 \pm 0.01	0.23 \pm 0.01	0.73 \pm 0.01	12.37''
70	05:05:44.20	-67:52:39.36	22.00 \pm 0.01	21.77 \pm 0.01	21.34 \pm 0.01	0.24 \pm 0.01	0.42 \pm 0.01	12.40''
71	05:05:40.10	-67:52:47.54	23.19 \pm 0.01	22.90 \pm 0.01	22.21 \pm 0.01	0.28 \pm 0.01	0.69 \pm 0.01	12.45''
72	05:05:41.46	-67:52:29.49	21.88 \pm 0.01	21.68 \pm 0.01	20.94 \pm 0.01	0.20 \pm 0.01	0.74 \pm 0.01	12.53''

TABLE 6 — Continued

Star	R.A. (J2000)	Decl. (J2000)	B	V	I	B-V	V-I	r
73	05:05:39.85	-67:52:43.92	22.71 \pm 0.01	22.48 \pm 0.01	21.81 \pm 0.01	0.23 \pm 0.01	0.67 \pm 0.01	12.60''
74	05:05:40.03	-67:52:35.92	21.92 \pm 0.01	21.56 \pm 0.01	20.55 \pm 0.01	0.36 \pm 0.01	1.01 \pm 0.01	12.68''
75	05:05:41.82	-67:52:54.28	21.21 \pm 0.01	21.09 \pm 0.00	20.71 \pm 0.01	0.11 \pm 0.01	0.39 \pm 0.01	12.76''
76	05:05:43.01	-67:52:53.10	23.13 \pm 0.01	22.80 \pm 0.01	22.04 \pm 0.01	0.33 \pm 0.01	0.76 \pm 0.01	12.76''
77	05:05:40.71	-67:52:51.95	21.67 \pm 0.01	21.57 \pm 0.01	21.17 \pm 0.01	0.10 \pm 0.01	0.40 \pm 0.01	12.80''
78	05:05:40.60	-67:52:51.86	22.63 \pm 0.01	22.39 \pm 0.01	21.83 \pm 0.01	0.23 \pm 0.01	0.57 \pm 0.01	13.11''
79	05:05:39.89	-67:52:46.50	22.18 \pm 0.01	21.96 \pm 0.01	21.35 \pm 0.01	0.22 \pm 0.01	0.61 \pm 0.01	13.12''
80	05:05:43.32	-67:52:30.53	19.69 \pm 0.00	19.25 \pm 0.00	18.19 \pm 0.00	0.44 \pm 0.00	1.06 \pm 0.00	13.19''
81	05:05:43.86	-67:52:33.28	21.31 \pm 0.01	21.12 \pm 0.00	20.78 \pm 0.01	0.18 \pm 0.01	0.35 \pm 0.01	13.21''
82	05:05:44.37	-67:52:39.22	22.50 \pm 0.01	22.29 \pm 0.01	21.72 \pm 0.01	0.20 \pm 0.01	0.57 \pm 0.01	13.39''
83	05:05:39.94	-67:52:47.93	19.86 \pm 0.00	19.78 \pm 0.00	19.63 \pm 0.00	0.08 \pm 0.00	0.15 \pm 0.00	13.44''
84	05:05:44.45	-67:52:42.42	22.28 \pm 0.01	22.02 \pm 0.01	21.39 \pm 0.01	0.26 \pm 0.01	0.63 \pm 0.01	13.63''
85	05:05:39.70	-67:52:37.64	23.22 \pm 0.01	22.92 \pm 0.01	22.27 \pm 0.01	0.30 \pm 0.01	0.65 \pm 0.01	13.78''
86	05:05:41.86	-67:52:55.72	23.05 \pm 0.01	22.76 \pm 0.01	22.06 \pm 0.01	0.29 \pm 0.01	0.70 \pm 0.01	14.18''
87	05:05:41.05	-67:52:54.66	22.72 \pm 0.01	22.46 \pm 0.01	21.84 \pm 0.01	0.26 \pm 0.01	0.63 \pm 0.01	14.23''
88	05:05:39.52	-67:52:40.34	22.65 \pm 0.01	22.41 \pm 0.01	21.69 \pm 0.01	0.24 \pm 0.01	0.72 \pm 0.01	14.28''
89	05:05:41.85	-67:52:27.29	21.12 \pm 0.01	20.89 \pm 0.00	20.21 \pm 0.01	0.23 \pm 0.01	0.67 \pm 0.01	14.33''

TABLE 7
FITTING STELLAR PARAMETERS OF THE STARS BRIGHTER THAN $V = 21.6$
MAG IN TABLE 6

Star	T_{eff} (K)	$\log g$ (dex)	[Fe/H] (dex)	V_r (km s $^{-1}$)
9	7222 \pm 200	4.1 \pm 1.0	-0.7 \pm 0.2	252 \pm 0
12	7202 \pm 201	3.7 \pm 1.0	-0.8 \pm 0.2	288 \pm 0
18	7090 \pm 201	3.8 \pm 1.0	-0.9 \pm 0.2	247 \pm 0
19	6710 \pm 201	4.2 \pm 1.0	-0.5 \pm 0.2	266 \pm 0
20	7418 \pm 201	4.5 \pm 1.0	-0.6 \pm 0.2	260 \pm 0
21	9181 \pm 200	3.9 \pm 1.0	-0.8 \pm 0.2	301 \pm 0
22	7698 \pm 201	4.3 \pm 1.0	-0.4 \pm 0.2	285 \pm 0
24	5783 \pm 200	4.3 \pm 1.0	-0.4 \pm 0.2	245 \pm 0
27	7549 \pm 200	4.4 \pm 1.0	-0.3 \pm 0.2	273 \pm 0
28	7044 \pm 200	4.1 \pm 1.0	-0.7 \pm 0.2	273 \pm 0
30	7411 \pm 201	4.3 \pm 1.0	-0.2 \pm 0.2	263 \pm 0
34	7733 \pm 201	4.3 \pm 1.0	-0.7 \pm 0.2	317 \pm 0
36	5612 \pm 202	4.2 \pm 1.0	-0.7 \pm 0.2	254 \pm 0
37	5613 \pm 200	3.8 \pm 1.0	-0.3 \pm 0.2	254 \pm 0
38	7692 \pm 201	4.0 \pm 1.0	-0.7 \pm 0.2	276 \pm 0
42	7338 \pm 200	3.9 \pm 1.0	-0.7 \pm 0.2	290 \pm 0
43	7201 \pm 201	3.1 \pm 1.0	-0.7 \pm 0.2	319 \pm 0
45	8051 \pm 200	4.3 \pm 1.0	-0.4 \pm 0.2	273 \pm 0
49	7145 \pm 201	3.8 \pm 1.0	-1.0 \pm 0.2	261 \pm 0
51	12780 \pm 200	4.7 \pm 1.0	-1.0 \pm 0.2	264 \pm 0
53	8699 \pm 201	3.9 \pm 1.0	-0.9 \pm 0.2	289 \pm 0
60	4846 \pm 200	3.0 \pm 1.0	-0.6 \pm 0.2	278 \pm 0
61	7032 \pm 201	3.9 \pm 1.0	-0.8 \pm 0.2	250 \pm 0
62	5862 \pm 200	3.8 \pm 1.0	-1.0 \pm 0.2	297 \pm 0
63	7883 \pm 201	4.7 \pm 1.0	0.2 \pm 0.2	287 \pm 0
74	6203 \pm 201	5.0 \pm 1.0	-0.2 \pm 0.2	252 \pm 0
75	7961 \pm 201	4.3 \pm 1.0	-0.4 \pm 0.2	281 \pm 0
77	7688 \pm 201	4.5 \pm 1.0	-0.5 \pm 0.2	245 \pm 0
80	5341 \pm 200	2.8 \pm 1.0	-0.6 \pm 0.2	213 \pm 0
81	7944 \pm 201	4.1 \pm 1.0	-0.4 \pm 0.2	264 \pm 0
83	10782 \pm 201	4.4 \pm 1.0	0.7 \pm 0.2	281 \pm 0
89	6273 \pm 200	3.5 \pm 1.0	-0.9 \pm 0.2	257 \pm 0

See the note in Table 5.

We have used photometric and spectroscopic methods to search for surviving companions in three young LMC Type Ia SNRs: 0519–69.0, DEM L71 and 0548–70.4. Below we discuss the pros and cons of these two methods in Subsections 7.1 and 7.2, and further discuss the inadequacy of Gaia Data in the search for surviving companions in Subsection 7.3. Finally, we discuss implications of our results on progenitor systems of Type Ia SNe.

7.1. Photometric Search

To probe the parameter space of a close non-degenerate companion of a WD that leads to a Type Ia SN of SD origin, detailed models of binary stellar evolution for a range of separations, mass ratios, and WD masses have been calculated (Hachisu et al. 1999; Han & Podsiadlowski 2004; Meng et al. 2007; Hachisu et al. 2008; Han 2008; Wang et al. 2009; Wang & Han 2009; Meng et al. 2009; Wang & Han 2010); however, most of these models end at the SN explosion without extending to the SN

impact on the stellar companion and afterwards. On the other hand, some hydrodynamic model calculations start from the Type Ia SN explosion and focus on the impact of SN ejecta on the surviving stellar companion and its subsequent evolution, taking into consideration of explosion geometry and impact angle (Marietta et al. 2000; Pakmor et al. 2008; Liu et al. 2012; Pan et al. 2014). In addition, less sophisticated calculations assuming ad hoc energy input and mass stripping have been made for the post-impact evolution of a $1 M_{\odot}$ subgiant or MS surviving companions (Podsiadlowski 2003; Shappee et al. 2013).

Among the above models, Pan et al. (2014) have carried out comprehensive calculations that detail the post-impact evolution of a surviving companion’s effective temperature and luminosity. They considered only MS and helium star companions. For a given temperature and luminosity of a surviving companion, its stellar emission was approximated by a blackbody model and convolved with a filter response curve to compute the photometric magnitude in that filter. Thus, the post-impact evolution of a surviving companion in the temperature-luminosity domain could be easily plotted in CMDs for direct comparisons with observations.

Using *HST* photometric measurements of stars in SNRs 0519–69.0, DEM L71, and 0548–70.4, we have constructed CMDs in V versus $B - V$ and I versus $V - I$, and compared the stars with Pan et al. (2014) evolutionary tracks of surviving MS and helium star companions (Figures 6, 12, and 20). We do not find any MS or helium star candidates with $V < 23.0$ for surviving companion in these three Type Ia SNRs. As Pan et al. (2014) did not model cases with RG companions, we cannot assess the existence of surviving RG companions in these SNRs, although there are a number of stars within our search radii lie on the RG branch in the CMDs. As shown by spectroscopic observations and discussed in the next subsection, some RG stars appear to show large peculiar radial velocities. Future models of surviving RG companions are needed for comparison.

Interestingly, in the SNR 0548–70.4, we find star 11 within the MS search radius in a strange location in the CMDs (Figure 20). Its colors cannot be reproduced by stars of any temperature with a normal extinction law. As there are additional sources with similar colors and location in the CMDs (e.g., star 770 and star 934), and the colors are similar to some cataloged galaxies, we think star 11 is most likely a background galaxy, instead of a star, as well as source 934. Unfortunately, star 11 is below the detection limit of the 2MASS catalog; future sensitive *JHK* photometric measurements are needed to extend its spectral energy distribution (SED) to confirm its nature as a background galaxy.

7.2. Peculiar Radial Velocity Search

We have also used VLT MUSE observations to carry out spectroscopic analyses, and used stellar spectra to search for high radial velocities as diagnostics of surviving companions. In the SNRs 0519–69.0 and DEM L71, we find each has a star with radial velocity that deviate by more than 2.5σ (75 and 50 km s^{-1}) from the mean of the underlying stellar population, 264 km s^{-1} and 270 km s^{-1} , respectively (see Figure 7 and Figure 15). These peculiar radial velocities are intriguing and may suggest

that these stars are surviving companions. In the case of 0519–69.0, star 5 is half way between the MS and helium star search radii, while in the case of DEM L71, star 80 is close to the helium star search radius; however, both stars with peculiar radial velocities are located in the RG branch in the CMDs. Because of the uncertainties in the exact site of SN explosion and our inadequate understanding of the Type Ia SN progenitors, we can neither confirm nor exclude these two stars as candidates for surviving companions in SNRs 0519–69.0 and DEM L71. Note that DEM L71 has two other stars with radial velocities at $> 2\sigma$ but $< 2.5\sigma$ from the mean radial velocity of the underlying population, and both their locations appear to be in the MS in the CMDs. Follow-up observations to measure chemical abundance and stellar rotation of these stars are needed to determine whether they are indeed surviving companions of Type Ia SN progenitors.

7.3. Peculiar Proper Motion Search

Beside the aforementioned methods, we have also looked into Gaia Data Release 2 (DR2) to investigate proper motions of stars near the explosion sites of the three SNRs, and search for large proper motions to diagnose surviving companions. A transverse velocity of 300 km s^{-1} at the LMC distance of $\sim 50 \text{ kpc}$ corresponds to a proper motion of 1.26 mas yr^{-1} . Most stars observed in these Type Ia SNRs are fainter than $V = 18-19$. As the quoted uncertainty in proper motion in Gaia DR2 is 1.20 mas yr^{-1} for a star with $G = 20$, it would be impossible to use Gaia DR2 to conduct a meaningful investigation of peculiar proper motions of intermediate- and low-mass stars. Stars near the tip of the RG branch are bright enough to have more accurate proper motion measurements, but no such RGs are seen in these Type Ia SNRs.

7.4. Implications for Type Ia SNe Progenitors

In the SD scenario, the companion of the WD progenitor is expected to survive the SN explosion and be identifiable (Marietta et al. 2000; Pakmor et al. 2008; Liu et al. 2013; Pan et al. 2014); however, recent searches of surviving companion in the Milky Way (MW) (Ruiz-Lapuente et al. 2004; Kerzendorf et al. 2009; González Hernández et al. 2009, 2012; Kerzendorf et al. 2012, 2013, 2014, 2018a,b; Ruiz-Lapuente et al. 2018b, 2019) and the LMC (Schaefer et al. 2012, EPS2012, PS2015, Li et al. 2017, Litke et al. 2017) have not unambiguously identified and confirmed any surviving companion. In this study, we have used photometric and spectroscopic methods to search for candidates of surviving companion within the three young LMC Type Ia SNRs, but are still unable to make unambiguous identification and confirmation. See Appendix A for a detailed compilation of these searches and their results.

Nevertheless, the lack of an obvious surviving companion cannot exclude the SD scenario. In the SD scenario, the modeled post-impact properties of surviving companion are usually calculated under reasonable assumptions for a simplified condition. It is conceivable that the assumed conditions are not appropriate and lead to discrepancies between the observations and model predictions of surviving companions. For instance, models of

Pan et al. (2014) adopt a classical SD scenario, in which a normal Chandrasekhar mass model (Whelan & Iben 1973; Nomoto 1982) with an initial spherically symmetric explosion is assumed. If the WD in the SD case has a sub-Chandrasekhar mass instead, and explodes through double detonation (Nomoto 1982), the explosion energy will be lower than that assumed by Pan et al. (2014). Furthermore, the SN explosion may not be spherically symmetric, as a result of the binary orbit and stellar rotation (Kashi & Soker 2011). These different explosion energy and geometry will certainly affect the post-impact temperature and luminosity of the surviving companions and change their locations in the CMDs. Future post-impact evolution models of surviving companions need to consider different types of SN explosions and, more importantly, include RG companions.

It should be noted that the conventional SD and DD classifications of Type Ia SNe may be an oversimplification. Many alternative models for Type Ia SNe have been proposed (see Wang & Han 2012; Maoz et al. 2014; Ruiz-Lapuente 2014; Wang 2018; Ruiz-Lapuente 2018a for reviews), such as the sub-Chandrasekhar model (Nomoto 1982; Woosley et al. 1986; Bildsten et al. 2007; Shen & Bildsten 2009; Fink et al. 2010; Guillochon et al. 2010; Dan et al. 2011; Raskin et al. 2012; Pakmor et al. 2013; Shen et al. 2018), the super-Chandrasekhar model (Yoon & Langer 2004; Hachisu et al. 2012a,b; Boshkayev et al. 2013; Wang et al. 2014), the spin-up/spin-down model (Di Stefano et al. 2011; Justham 2011), the single-star model (Iben & Renzini 1983; Tout et al. 2008), the violent DD merger model (Pakmor et al. 2010, 2011, 2012), the collisional DD model (Chomiuk et al. 2008; Raskin et al. 2009; Kushnir et al. 2013), the core-degenerate (CD) model (Kashi & Soker 2011), and the M-dwarf model (Wheeler 2012), etc. These models predict different outcomes for Type Ia SNe apart from the classical SD scenario, resulting in different geometric distribution and abundance of the SN ejecta whose impact on a surviving companion would manifest differently and need further exploration.

Finally, from studies of the five young Balmer-dominated Type Ia SNRs in the LMC, we find: no surviving stellar companion exists in 0509–67.5 (Schaefer et al. 2012; Litke et al. 2017); Star 1 in N103B is a promising candidate for surviving companion (Li et al. 2017); 0548–70.4 has no obvious candidate for surviving companion, while DEM L71 and 0519–69.0 each has a possible candidate for surviving companion based on anomalous radial velocities (this paper). These results imply 20% – 60% of them may originate from SD Type Ia SNe. This is not inconsistent with the 20% suggested by González Hernández et al. (2012); however, these results are derived with small number statistics. Future surveys of young Balmer-dominated Type Ia SNRs in nearby galaxies, such as M31 and M33, should be made in order to expand the Type Ia SNR sample size and the 30m-class telescopes under construction can be used to search for surviving companions of Type Ia SNe in the future.

8. SUMMARY

We have been searching for surviving companions of Type Ia SN progenitors in five SNRs in the LMC. This paper reports our study of three Type Ia SNRs in the LMC: 0519–69.0, DEM L71, and 0548–70.4.

We used our and archival *HST* images in $H\alpha$ and *BVI* continuum bands to examine structures of the SNRs and their underlying stellar populations, respectively. The continuum-band images were used to make photometric measurements and construct CMDs for stars projected in the SNRs and their vicinities, in order to be compared with model predictions of post-impact evolution of surviving companions.

All stars within a search radius from an estimated SN explosion site were considered initially. To find the sites of SN explosion, we fitted ellipses to the SNRs’ Balmer shells and adopted the centers of the ellipses as the SN explosion sites. The search radii were adopted from the runaway distances for surviving MS and He star companions, estimated as SNR age times possible kick velocities.

The faintest post-impact surviving companions in the models of Pan et al. (2014) have $V \sim 23.0$ mag for He star companions; thus we only include stars with $V < 23.0$ in the CMDs for comparisons with models. In these comparisons we do not find any star located on post-impact evolutionary tracks consistently between the V versus $B - V$ and I versus $V - I$ CMDs. Note that the explosion mechanism and geometry maybe different from those assumed by Pan et al. (2014); thus, our search cannot exclude faint companions that were not considered by Pan et al. (2014).

We have also used VLT MUSE observations of 0519–69.0 and DEM L71 to perform spectroscopic analyses of the stars with $V < 21.6$ mag in each SNR to search for peculiar radial velocities as diagnostic for candidate surviving companions. We find one star in each SNR with radial velocity offset from the mean velocity of the underlying stellar population, $264\text{--}270\text{ km s}^{-1}$, by more than 2.5σ ($75\text{--}50\text{ km s}^{-1}$). Both stars with large peculiar radial velocities are RG stars. These stars need to be investigated further for abundance anomaly to confirm their surviving companion status.

As compiled in Appendix A, the number of Type Ia SNRs in which surviving companions have been searched is too small for statistically significant conclusions. More young Type Ia SNRs in nearby galaxies, such as M31 and M33, need to be surveyed to enlarge the sample for searches of surviving companions using 30m-class telescopes in the future.

We thank Dr. Thomas Krühler for his help with the VLT MUSE data reduction. This project is supported by the NASA grant HST-GO-13282.01-A. Y.-H.C. and C.-J.L. are supported by Taiwanese Ministry of Science and Technology grant MOST 108-2811-M-001-587. K.-C.P. is supported by the MOST grant MOST 107-2112-M-007-032-MY3. T.-W.C. acknowledges the funding provided by the Alexander von Humboldt Foundation. The Programme IDs of VLT MUSE data acquired at ESO are 096.D-0352(A) and 096.D-0352(A).

APPENDIX APPENDIX A

TABLE 8
A DETAILED, UP-TO-DATE COMPILATION OF SEARCHES FOR TYPE IA SN PROGENITORS'S SURVIVING COMPANIONS IN GALACTIC
AND LMC SNRS

Galaxy/SNR	Reference	Observations	Companion Candidate	Diagnostics	Result*	Progenitors (WD + ?)
MW/Tycho	Ruiz-Lapuente et al. (2004) (RLCM04)	<i>Photometry and astrometry:</i> HST WFPC2 F555W, F675W. <i>Spectroscopy:</i> WHT 4.2 m UES and ISIS, NOT 2.5 m ALFOSC, Keck I 10 m ESI and LRIS, Keck II 10 m LRIS	Tycho G	Radial velocity and proper motion	+	SD (WD+Tycho G). RG excluded.
.	Fuhrmann (2005)	Radial velocity, proper motion and distance from RLCM04	Tycho G	The kinematics in Toomre diagram	−	.
.	Ihara et al. (2007)	<i>Photometry:</i> Subaru 8.2 m Suprime-Cam V , R_C , I_C . <i>Spectroscopy:</i> Subaru 8.2 m FOCAS/MOS	Tycho G	Blueshifted Fe I absorption by the SN ejecta	−	SD (WD+Tycho E)
.	González Hernández et al. (2009)	<i>Spectroscopy:</i> Keck I 10 m HIRES and LRIS	Tycho G	Nickel (Ni) and cobalt (Co) abundances	+	SD (WD+Tycho G)
.	Kerzendorf et al. (2009)	<i>Astrometry:</i> Palomar 5.1 m, INT 2.5 m <i>Spectroscopy:</i> Subaru 8.2 m HDS	Tycho G	Radial velocity, distance, stellar parameters, rotational velocity and proper motion	−	.
.	Lu et al. (2011)	<i>X-ray imaging:</i> Chandra ACIS	Tycho G	Proper motion and X-ray morphology	+	SD
.	Kerzendorf et al. (2013)	<i>Astrometry:</i> HST ACS/WFC F555W <i>Spectroscopy:</i> Keck I 10 m HIRES and LRIS	Tycho G	Ni abundance, radial velocity, distance, rotational velocity and proper motion	−	Non-classical SD or DD (WD+WD)
.	Bedin et al. (2014) (BRLGH14)	<i>Photometry and astrometry:</i> HST ACS/WFC F555W, WFC3/UVIS F555W. <i>Spectroscopy:</i> Keck I 10 m HIRES, La Silla 3.6 m HARPS	Tycho G	Proper motion, metallicity and Ni abundance	+	SD (WD+Tycho G) or DD (WD+WD)
.	Xue & Schaefer (2015)	<i>Astrometry:</i> 42 observations from seven astronomers.	Tycho G	Position in the SNR	−†	.
.	Ruiz-Lapuente et al. (2019)	<i>Photometry and astrometry:</i> Gaia DR2. Photometry, astrometry and radial velocity from BRLGH14.	Tycho G	Galactic orbital kinematics and metallicity	+	SD (WD+Tycho G) or DD (WD+WD) or CD (WD+AGB)
MW/Tycho	Ihara et al. (2007)	<i>Photometry:</i> Subaru 8.2 m Suprime-Cam V , R_C , I_C . <i>Spectroscopy:</i> Subaru 8.2 m FOCAS/MOS	Tycho E	Blueshifted Fe I absorption by the SN ejecta	+	SD (WD+Tycho E)
.	González Hernández et al. (2009)	<i>Spectroscopy:</i> Keck I 10 m HIRES and LRIS	Tycho E	A double-lined spectroscopic binary	−	SD (WD+Tycho G)
.	Kerzendorf et al. (2009)	<i>Astrometry:</i> Palomar 5.1 m, INT 2.5 m <i>Spectroscopy:</i> Subaru 8.2 m HDS	Tycho E	Radial velocity and proper motion	−	.
.	Kerzendorf et al. (2013)	<i>Astrometry:</i> HST ACS/WFC F555W <i>Spectroscopy:</i> Keck I 10 m HIRES and LRIS	Tycho E	Radial velocity, rotational velocity, proper motion and distance	−	Non-classical SD or DD (WD+WD)
.	Xue & Schaefer (2015)	<i>Astrometry:</i> 42 observations from seven astronomers.	Tycho E	Position in the SNR	−†	.
.	Ruiz-Lapuente et al. (2019)	<i>Photometry and astrometry:</i> Gaia DR2. Photometry, astrometry and radial velocity from BRLGH14	Tycho E	Distance	−	SD (WD+Tycho G) or DD (WD+WD) or CD (WD+AGB)
MW/Tycho	Kerzendorf et al. (2013)	<i>Astrometry:</i> HST ACS/WFC F555W <i>Spectroscopy:</i> Keck I 10 m HIRES and LRIS	Tycho B	Radial velocity and proper motion Temperature, rotational velocity, abundance, and position in the SNR +	Non-classical SD or DD (WD+WD)
.	Bedin et al. (2014) (BRLGH14)	<i>Photometry and astrometry:</i> HST ACS/WFC F555W, WFC3/UVIS F555W. <i>Spectroscopy:</i> Keck I 10 m HIRES, La Silla 3.6 m HARPS	Tycho B	Rotational velocity, radial velocity, and proper motion	−	SD (WD+Tycho G) or DD (WD+WD)
.	Xue & Schaefer (2015)	<i>Astrometry:</i> 42 observations from seven astronomers.	Tycho B	Position in the SNR	−†	.
.	Kerzendorf et al. (2018b)	<i>Spectroscopy:</i> HST STIS	Tycho B	Fe II absorption by cold SN ejecta in the UV spectra and the luminosity distance	−	Non-classical SD
.	Ruiz-Lapuente et al. (2019)	<i>Photometry and astrometry:</i> Gaia DR2. Photometry, astrometry and radial velocity from BRLGH14	Tycho B	Radial velocity and proper motion	−	SD (WD+Tycho G) or DD (WD+WD) or CD (WD+AGB)
MW/SN 1006	González Hernández et al. (2012)	<i>Photometry:</i> 2MASS R , B , J , H , K . <i>Spectroscopy:</i> VLT-UT2 Kueyen 8.2 m UVES	None	Radial velocity, rotational velocity, distance, and abundances	−	SD (WD+MS< M_{\odot}) or DD (WD+WD)
.	Kerzendorf et al. (2012)	<i>Photometry:</i> ANU 2.3 m Imager U , B , V , I . <i>Spectroscopy:</i> VLT-UT2 FLAMES	None	Radial velocity, rotational velocity, and stellar parameters	−	Non-classical SD or DD (WD+WD)
.	Kerzendorf et al. (2018a)	<i>Photometry:</i> CTIO Blanco 4 m DECam u , g , r , z	None	WD models in CMD	−	Non-classical progenitors (WD+anomalously red/dim WD) or DD (WD+WD). Young WDs models $\leq 10^8$ yr excluded
MW/Kepler	Kerzendorf et al. (2014)	<i>Photometry:</i> HST ACS/WFC F550M, NOMAD catalog B , V , R , J , H , K . <i>Spectroscopy:</i> ANU 2.3 m WiFeS	Many	Radial velocity and stellar luminosity	?	RG excluded

TABLE 8 — Continued

Galaxy/SNR	Reference	Observations	Companion Candidate	Diagnostics	Result *	Progenitors (WD + ?)
.	Ruiz-Lapuente et al. (2018b)	<i>Photometry and astrometry: HST ACS/WFC F502N, F660N, F658N, F550M, WFC3/UVIS F336W, F438W, F547M, F656N, F658N, F814W. Spectroscopy: VLT-UT2 FLAMES UVES and Giraffe</i>	None	Radial velocity, rotational velocity, and proper motion	—	DD (WD+WD) or CD (WD+AGB)
LMC/SNR 0509-67.5	Schaefer et al. (2012)	<i>SNR imaging: HST WFPC2 F656N, Chandra ACIS. Photometry: HST WFC3/UVIS F475W, F555W, F814W</i>	None	Stellar luminosity	—	DD (WD+WD)
.	Hovey (2016)	<i>SNR imaging: HST ACS/WFC F656N. Photometry: HST WFC3/UVIS F110W, F160W, F475W, F555W, F814W</i>	Many	Position in the SNR and stellar color and luminosity	?	SD not excluded
.	Litke et al. (2017)	<i>SNR imaging: HST ACS/WFC F658N, WFPC2 F656N. Photometry: HST WFC3/UVIS F475W, F555W, F814W, WFC3/IR F110W, F160W, Spitzer IRAC 3.6, 4.5, 5.8, 8.0 μm</i>	None	Models of surviving companions in CMDs	—	DD (WD+WD)
LMC/SNR 0519-69.0	Edwards et al. (2012)	<i>SNR imaging: HST ACS/WFC F658N, Chandra ACIS. Photometry: HST ACS/WFC F550M, F658N</i>	Many	Stellar color and luminosity	?	SD (WD+MS) or DD (WD+WD)
.	This paper	<i>SNR imaging: HST ACS/WFC F658N. Photometry: HST ACS/WFC F550M, WFC3/UVIS F475W, F814W. Spectroscopy: VLT-UT4 MUSE</i>	Star 5	Radial velocity and models of surviving companions in CMDs	+	SD (WD+star) or DD (WD+WD)
LMC/N103B	Pagnotta & Schaefer (2015)	<i>SNR imaging: Gemini 8.1 m GMOS Hα, Chandra ACIS, Australia Telescope. Photometry: Gemini 8.1 m GMOS g', r', i'</i>	Many	Stellar color and luminosity	?	SD (WD+star) or DD (WD+WD)
.	Li et al. (2017)	<i>SNR imaging: HST WFC3/UVIS F656N, CTIO Blanco 4 m MOSAIC II Hα. Photometry: HST WFC3/UVIS F475W, F555W, F814W. Spectroscopy: CTIO 4 m echelle, CTIO SMARTS 1.5 m CHIRON</i>	Star 1	Stellar colors and luminosity, models of surviving companions in CMDs, and position in the SNR	+	SD (WD+star)
LMC/DEM L71	Pagnotta & Schaefer (2015)	<i>SNR imaging: Gemini 8.1 m GMOS Hα, Chandra ACIS. Photometry: Gemini 8.1 m GMOS g', r', i'</i>	Many	Stellar color and luminosity	?	SD (WD+star) or DD (WD+WD)
.	This paper	<i>SNR imaging: HST WFC3/UVIS F656N. Photometry: HST WFC3/UVIS F475W, F555W, F814W. Spectroscopy: VLT-UT4 MUSE</i>	Star 80	Radial velocity and models of surviving companions in CMDs	+	SD (WD+star) or DD (WD+WD)
LMC/SNR 0548-70.4	This paper	<i>SNR imaging: HST WFC3/UVIS F656N. Photometry: HST WFC3/UVIS F475W, F555W, F814W</i>	Star 11	Models of surviving companions in CMDs	?	SD (WD+star) or DD (WD+WD)

* The symbol "+" and "-" represents a positive and negative result, respectively.

† See [Williams et al. \(2016\)](#) for discussions.

APPENDIX B

TABLE 9
STARS BRIGHTER THAN $V = 23.0$ MAG NEAR CENTRAL REGION IN THE SNR
0548–70.4

Star	R.A. (J2000)	Decl. (J2000)	B	V	I	B-V	V-I	r
1	05:47:48.339	-70:24:51.19	22.62 ± 0.01	22.32 ± 0.01	21.59 ± 0.01	0.30 ± 0.01	0.73 ± 0.01	1.39''
2	05:47:47.950	-70:24:53.02	22.81 ± 0.01	22.53 ± 0.01	21.81 ± 0.01	0.28 ± 0.01	0.72 ± 0.01	2.65''
3	05:47:48.004	-70:24:50.30	21.77 ± 0.01	21.55 ± 0.01	20.96 ± 0.01	0.22 ± 0.01	0.59 ± 0.01	3.14''
4	05:47:48.290	-70:24:49.32	22.37 ± 0.01	22.15 ± 0.01	21.55 ± 0.01	0.22 ± 0.01	0.60 ± 0.01	3.23''
5	05:47:47.951	-70:24:50.01	23.12 ± 0.01	22.87 ± 0.01	22.09 ± 0.01	0.25 ± 0.02	0.78 ± 0.02	3.54''
6	05:47:48.103	-70:24:55.48	21.64 ± 0.01	21.49 ± 0.01	21.03 ± 0.01	0.15 ± 0.01	0.46 ± 0.01	3.55''
7	05:47:48.863	-70:24:48.68	21.13 ± 0.01	21.03 ± 0.00	20.73 ± 0.01	0.10 ± 0.01	0.30 ± 0.01	4.25''
8	05:47:49.342	-70:24:52.83	23.13 ± 0.01	22.85 ± 0.01	22.05 ± 0.01	0.28 ± 0.02	0.80 ± 0.02	4.43''
9	05:47:47.979	-70:24:56.27	18.95 ± 0.00	18.56 ± 0.00	17.48 ± 0.00	0.39 ± 0.00	1.08 ± 0.00	4.55''
10	05:47:48.953	-70:24:48.59	22.87 ± 0.01	22.62 ± 0.01	21.89 ± 0.01	0.25 ± 0.01	0.73 ± 0.01	4.56''

* This table only contains a 10-line example. The full data that contains 973 data lines only appears in the machine readable format in the HTML.

REFERENCES

- Allard, F., & Hauschildt, P. H. 1995, *ApJ*, 445, 433
 Bauer, E. B., White, C. J., & Bildsten, L. 2019, arXiv e-prints, arXiv:1906.08941
 Bedin, L. R., Ruiz-Lapuente, P., González Hernández, J. I., et al. 2014, *MNRAS*, 439, 354
 Bildsten, L., Shen, K. J., Weinberg, N. N., & Nelemans, G. 2007, *ApJ*, 662, L95
 Blair, W. P., Long, K. S., & Vancura, O. 1991, *ApJ*, 366, 484
 Boshkayev, K., Rueda, J. A., Ruffini, R., et al. 2013, *ApJ*, 762, 117
 Canal, R., Méndez, J., & Ruiz-Lapuente, P. 2001, *ApJ*, 550, L53
 Chevalier, R. A., Kirshner, R. P., & Raymond, J. C. 1980, *ApJ*, 235, 186
 Chomiuk, L., Strader, J., & Brodie, J. P. 2008, *AJ*, 136, 234
 Dan, M., Rosswog, S., Guillochon, J., & Ramirez-Ruiz, E. 2011, *ApJ*, 737, 89
 Davies, R. D., Elliott, K. H., & Meaburn, J. 1976, *MmRAS*, 81, 89
 Dekker, H., D'Odorico, S., Kaufer, A., Delabre, B., & Kotzlowski, H. 2000, *Proc. SPIE*, 4008, 534
 Dennefeld, M. 1982, *A&A*, 112, 215
 Di Stefano, R., Voss, R., & Claeys, J. S. W. 2011, *ApJ*, 738, L1
 Dickel, J. R., & Milne, D. K. 1995, *AJ*, 109, 200
 Do, T., Martinez, G. D., Yelda, S., et al. 2013, *ApJ*, 779, L6
 Dolphin, A. E. 2000, *PASP*, 112, 1383
 Edwards, Z. I., Pagnotta, A., & Schaefer, B. E. 2012, *ApJ*, 747, L19
 Feroz, F., Hobson, M. P., & Bridges, M. 2009, *MNRAS*, 398, 1601
 Feldmeier-Krause, A., Kerzendorf, W., Neumayer, N., et al. 2017, *MNRAS*, 464, 194
 Fink, M., Röpke, F. K., Hillebrandt, W., et al. 2010, *A&A*, 514, A53
 Fuhrmann, K. 2005, *MNRAS*, 359, L35
 Geier, S., Marsh, T. R., Wang, B., et al. 2013, *A&A*, 554, A54
 Ghavamian, P., Rakowski, C. E., Hughes, J. P., & Williams, T. B. 2003, *ApJ*, 590, 833
 Ghavamian, P., Blair, W. P., Sankrit, R., Raymond, J. C., & Hughes, J. P. 2007, *ApJ*, 664, 304
 González Hernández, J. I., Ruiz-Lapuente, P., Filippenko, A. V., et al. 2009, *ApJ*, 691, 1
 González Hernández, J. I., Ruiz-Lapuente, P., Tabernero, H. M., et al. 2012, *Nature*, 489, 533
 Guillochon, J., Dan, M., Ramirez-Ruiz, E., & Rosswog, S. 2010, *ApJ*, 709, L64
 Hachisu, I., Kato, M., & Nomoto, K. 1999, *ApJ*, 522, 487
 Hachisu, I., Kato, M., & Nomoto, K. 2008, *ApJ*, 679, 1390-1404
 Hachisu, I., Kato, M., Saio, H., & Nomoto, K. 2012, *ApJ*, 744, 69
 Hachisu, I., Kato, M., & Nomoto, K. 2012, *ApJ*, 756, L4
 Han, Z. 2008, *ApJ*, 677, L109
 Han, Z., & Podsiadlowski, P. 2004, *MNRAS*, 350, 1301
 Hendrick, S. P., Borkowski, K. J., & Reynolds, S. P. 2003, *ApJ*, 593, 370
 Hook, I. M., Jørgensen, I., Allington-Smith, J. R., et al. 2004, *PASP*, 116, 425
 Hovey, L. 2016, Ph.D. Thesis
 Hughes, J. P., Hayashi, I., Helfand, D., et al. 1995, *ApJ*, 444, L81
 Hughes, J. P., Hayashi, I., & Koyama, K. 1998, *ApJ*, 505, 732
 Hughes, J. P., Ghavamian, P., Rakowski, C. E., & Slane, P. O. 2003, *ApJ*, 582, L95
 Iben, I., Jr., & Renzini, A. 1983, *ARA&A*, 21, 271
 Iben, I., Jr., & Tutukov, A. V. 1984, *ApJS*, 54, 335
 Ihara, Y., Ozaki, J., Doi, M., et al. 2007, *PASJ*, 59, 811
 Ivanova, N., & Taam, R. E. 2004, *ApJ*, 601, 1058
 Justham, S. 2011, *ApJ*, 730, L34
 Kamann, S., Wisotzki, L., & Roth, M. M. 2013, *A&A*, 549, A71
 Kashi, A., & Soker, N. 2011, *MNRAS*, 417, 1466
 Kerzendorf, W. E., Schmidt, B. P., Asplund, M., et al. 2009, *ApJ*, 701, 1665
 Kerzendorf, W. E., Schmidt, B. P., Laird, J. B., Podsiadlowski, P., & Bessell, M. S. 2012, *ApJ*, 759, 7
 Kerzendorf, W. E., Yong, D., Schmidt, B. P., et al. 2013, *ApJ*, 774, 99
 Kerzendorf, W. E., Childress, M., Scharwächter, J., Do, T., & Schmidt, B. P. 2013, *ApJ*, 782, 27
 Kerzendorf, W., & Do, T. 2015, Zenodo Source Code Library, doi: 10.5281/zenodo.28016
 Kerzendorf, W. E., Strampelli, G., Shen, K. J., et al. 2018, *MNRAS*, 479, 192
 Kerzendorf, W. E., Long, K. S., Winkler, P. F., & Do, T. 2018, *MNRAS*, 479, 5696
 Krühler, T., Kuncarayakti, H., Schady, P., et al. 2017, *A&A*, 602, A85
 Kushnir, D., Katz, B., Dong, S., Livne, E., & Fernández, R. 2013, *ApJ*, 778, L37
 Langer, N., Deutschmann, A., Wellstein, S., & Höflich, P. 2000, *A&A*, 362, 1046
 Lewis, K. T., Burrows, D. N., Hughes, J. P., et al. 2003, *ApJ*, 582, 770
 Li, C.-J., Chu, Y.-H., Gruendl, R. A., et al. 2017, *ApJ*, 836, 85
 Litke, K. C., Chu, Y.-H., Holmes, A., et al. 2017, *ApJ*, 837, 111
 Liu, Z. W., Pakmor, R., Röpke, F. K., et al. 2012, *A&A*, 548, A2
 Liu, Z.-W., Pakmor, R., Seitenzahl, I. R., et al. 2013, *ApJ*, 774, 37
 Lu, F. J., Wang, Q. D., Ge, M. Y., et al. 2011, *ApJ*, 732, 11
 Maoz, D., Mannucci, F., & Nelemans, G. 2014, *ARA&A*, 52, 107
 Marietta, E., Burrows, A., & Fryxell, B. 2000, *ApJS*, 128, 615
 Martínez-Rodríguez, H., Badenes, C., Lee, S.-H., et al. 2018, *ApJ*, 865, 151
 Meng, X., Chen, X., & Han, Z. 2007, *PASJ*, 59, 835
 Meng, X., Chen, X., & Han, Z. 2009, *MNRAS*, 395, 2103
 Nikolaev, S., Drake, A. J., Keller, S. C., et al. 2004, *ApJ*, 601, 260
 Nomoto, K. 1982, *ApJ*, 257, 780
 Olsen, K. A. G., & Salyk, C. 2002, *AJ*, 124, 2045
 Ou, P.-S., Chu, Y.-H., Maggi, P., et al. 2018, *ApJ*, 863, 137
 Pagnotta, A., Walker, E. S., & Schaefer, B. E. 2014, *ApJ*, 788, 173
 Pagnotta, A., & Schaefer, B. E. 2015, *ApJ*, 799, 101
 Pakmor, R., Röpke, F. K., Weiss, A., & Hillebrandt, W. 2008, *A&A*, 489, 943
 Pakmor, R., Kromer, M., Röpke, F.K., et al. 2010, *Nature* 463, 61
 Pakmor, R., Hachinger, S., Röpke, F.K., Hillebrandt, W., 2011, *A&A*, 528, A117
 Pakmor, R., Kromer, M., Taubenberger, S., Sim, S.A., Röpke, F.K., Hillebrandt, W., 2012, *ApJ* 747, L10
 Pakmor, R., Kromer, M., Taubenberger, S., & Springel, V. 2013, *ApJ*, 770, L8
 Pan, K.-C., Ricker, P. M., & Taam, R. E. 2010, *ApJ*, 715, 78
 Pan, K.-C., Ricker, P. M., & Taam, R. E. 2012, *ApJ*, 750, 151
 Pan, K.-C., Ricker, P. M., & Taam, R. E. 2012, *ApJ*, 760, 21

- Pan, K.-C., Ricker, P. M., & Taam, R. E. 2013, *ApJ*, 773, 49
- Pan, K.-C., Ricker, P. M., & Taam, R. E. 2014, *ApJ*, 792, 71
- Pietrzyński, G., Graczyk, D., Gieren, W., et al. 2013, *Nature*, 495, 76
- Pietrzyński, G., Graczyk, D., Gallenne, A., et al. 2019, *Nature*, 567, 200
- Podsiadlowski, P. 2003, [arXiv:astro-ph/0303660](https://arxiv.org/abs/astro-ph/0303660)
- Rakowski, C. E., Ghavamian, P., & Hughes, J. P. 2003, *ApJ*, 590, 846
- Raskin, C., Timmes, F. X., Scannapieco, E., Diehl, S., & Fryer, C. 2009, *MNRAS*, 399, L156
- Raskin, C., Scannapieco, E., Fryer, C., Rockefeller, G., & Timmes, F. X. 2012, *ApJ*, 746, 62
- Rest, A., Suntzeff, N. B., Olsen, K., et al. 2005, *Nature*, 438, 1132
- Rest, A., Matheson, T., Blondin, S., et al. 2008, *ApJ*, 680, 1137-1148
- Ruiz-Lapuente, P. 1997, *Science*, 276, 1813
- Ruiz-Lapuente, P., Comeron, F., Méndez, J., et al. 2004, *Nature*, 431, 1069
- Ruiz-Lapuente, P. 2014, *NewAR*, 62, 15
- Ruiz-Lapuente, P. 2018, *arXiv e-prints*, [arXiv:1812.04977](https://arxiv.org/abs/1812.04977)
- Ruiz-Lapuente, P., Damiani, F., Bedin, L., et al. 2018, *ApJ*, 862, 124
- Ruiz-Lapuente, P., González Hernández, J. I., Mor, R., et al. 2019, *ApJ*, 870, 135
- Russell, S. C., & Dopita, M. A. 1992, *ApJ*, 384, 508
- Sano, H., Yamane, Y., Tokuda, K., et al. 2018, *ApJ*, 867, 7
- Shappee, B. J., Kochanek, C. S., & Stanek, K. Z. 2013, *ApJ*, 765, 150
- Schaefer, B. E., & Pagnotta, A. 2012, *Nature*, 481, 7380
- Shen, K. J., & Bildsten, L. 2009, *ApJ*, 699, 1365
- Shen, K. J., Boubert, D., Gänsicke, B. T., et al. 2018, *ApJ*, 865, 15
- Smith, R. C., Kirshner, R. P., Blair, W. P., & Winkler, P. F. 1991, *ApJ*, 375, 652
- Soto, K. T., Lilly, S. J., Bacon, R., Richard, J., & Conseil, S. 2016, *MNRAS*, 458, 3210
- Støstad, M., Do, T., Murray, N., et al. 2015, *ApJ*, 808, 106
- Tout, C. A., Wickramasinghe, D. T., & Lattanzio, J. C. 2008, *Evolution and Nucleosynthesis in AGB Stars*, 1001, 25
- Tuohy, I. R., Dopita, M. A., Mathewson, D. S., Long, K. S., & Helfand, D. J. 1982, *ApJ*, 261, 473
- Van den Bergh, S., Marscher, A. P., & Terzian, Y. 1973, *ApJS*, 26, 19
- Van den Bergh, S., & Kamper, K. W. 1977, *ApJ*, 218, 617
- van der Marel, R. P., & Cioni, M.-R. L. 2001, *AJ*, 122, 1807
- van Kerkwijk, M. H., Chang, P., Justham, S., 2010. *ApJ* 722, L157
- Villaver, E., Manchado, A., & García-Segura, G. 2012, *ApJ*, 748, 94
- Wang, B., Meng, X., Chen, X., & Han, Z. 2009, *MNRAS*, 395, 847
- Wang, B., & Han, Z. 2009, *A&A*, 508, L27
- Wang, B., & Han, Z. 2010, *MNRAS*, 404, L84
- Wang, B., & Han, Z. 2012, *New A Rev.*, 56, 122
- Wang, B., Justham, S., Liu, Z.-W., et al. 2014, *MNRAS*, 445, 2340
- Wang, B. 2018, *Research in Astronomy and Astrophysics*, 18, 049
- Webbink, R. F. 1984, *ApJ*, 277, 355
- Weilbacher, P. M., Streicher, O., Urrutia, T., et al. 2014, in *ASP Conf. Ser.*, Vol. 485, *Astronomical Data Analysis Software and Systems XXIII*, ed. N. Manset & P. Forshay, 451
- Williams, B. J., Borkowski, K. J., Reynolds, S. P., et al. 2012, *ApJ*, 755, 3
- Williams, B. J., Borkowski, K. J., Reynolds, S. P., et al. 2014, *ApJ*, 790, 139
- Williams, B. F., Lang, D., Dalcanton, J. J., et al. 2014, *ApJS*, 215, 9
- Williams, B. J., Chomiuk, L., Hewitt, J. W., et al. 2016, *ApJ*, 823, L32
- Wheeler, J. C. 2012, *ApJ*, 758, 123
- Whelan, J., & Iben, I., Jr. 1973, *ApJ*, 186, 1007
- Woosley, S. E., Taam, R. E., & Weaver, T. A. 1986, *ApJ*, 301, 601
- Xue, Z., & Schaefer, B. E. 2015, *ApJ*, 809, 183
- Yamaguchi, H., Badenes, C., Petre, R., et al. 2014, *ApJ*, 785, L27
- Yoon, S.-C., & Langer, N. 2004, *A&A*, 419, 623
- Zaritsky, D., Harris, J., Thompson, I. B., & Grebel, E. K. 2004, *AJ*, 128, 1606